MICHIGAN STATE UNIVERSITY

CYCLOTRON LABORATORY

ELECTRIC QUADRUPOLE AND HEXADECUPOLE NUCLEAR EXCITATIONS FROM THE PERSPECTIVES OF ELECTRON SCATTERING AND MODERN SHELL-MODEL THEORY

B.A. BROWN, R. RADHI and B.H. WILDENTHAL

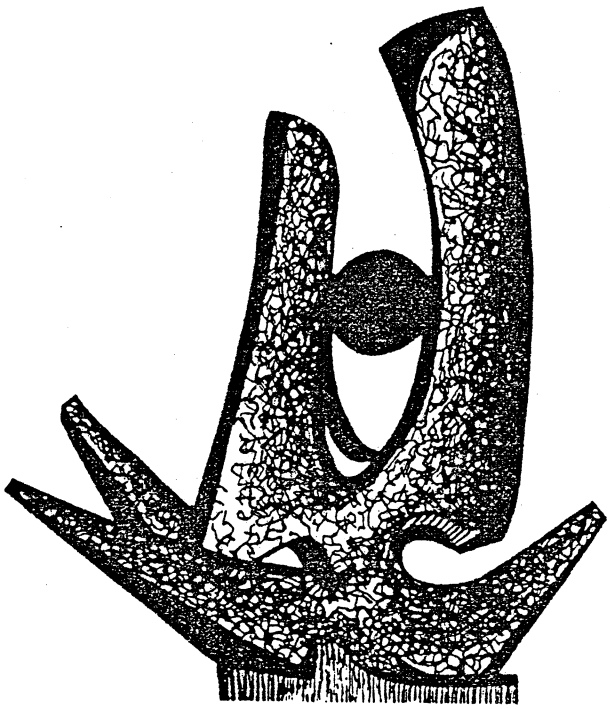

MAY 1983

MSUCL-415

MSUCL-415
May 1983

Electric quadrupole and hexadecupole nuclear excitations from the perspectives of electron scattering and modern shell-model theory

B. A. Brown, R. Radhi and B. H. Wildenthal

National Superconducting Cyclotron Laboratory
Michigan State University
East Lansing, Michigan 48824

ABSTRACT: Shell-model wave functions obtained from a complete, unified treatment of the structure of the positive parity states in nuclei between ^{16}O and ^{40}Ca are used to calculate the features of inelastic electron scattering to 2+ and 4+ states in this region. These predictions of E2 and E4 form factors, and the corresponding elastic scattering predictions, are compared with the collected experimental data which are available on this topic. The dependence of the calculated results upon alternate models for single-nucleon wave functions and core-polarization transition densities is investigated, as is the consistency between the (e,e') measuements and the analogous B(E2) measurements.

KEYWORDS:

[20Ne, 22Ne, 24Mg, 26Mg, 28Si, 30Si, 32S, 34S, 36Ar; calculated form factors for elastic electron scattering and longitudinal-electric inelastic electron scattering to 2+ and 4+ states; shell-model wave functions, complete $0d_{5/2}$-$1s_{1/2}$-$0d_{3/2}$ basis spaces, empirical, unified sd-shell model Hamiltonian.]

I. Introduction.

The electron is a probe which is uniquely well suited to reveal many aspects of nuclear structure. The general theory of its interaction with the constituents of the nucleus via the electromagnetic field is, of course, well understood (Ref 1, Ref 2, Ref 3). The relative weakness of this interaction makes it possible, moreover, to safely ignore in almost all instances the complications associated with multiple-step terms in a transition between the target and a final nuclear state. Hence, the cross sections associated with the population of a particular nuclear state can be interpreted cleanly in terms of the overlap between its wave function and that of the target.

Early experimental investigations of nuclear structure with electrons concentrated primarily on descriptions of the ground state charge distributions, via studies of elastic scattering (Ref 4). This line of research is still actively pursued (Ref 5), with measurements being extended to ever higher values of momentum transfer and, correspondingly, to ever finer details of the radial distribution of charge in the nucleus. In addition to providing information on the charge distribution, studies of the nuclear ground state with electron scattering techniques have now been extended to encompass the distribution of its magnetization and currents as well (Ref 6, Ref 7).

In addition to its power in characterizing the nuclear ground state, the technique of electron scattering also offers an unparalleled

avenue for exploration of transitions between nuclear states, via inelastic scattering (Ref 1, Ref 8, Ref 9, Ref 10).
A number of "low-energy" (40-120 MeV) electron accelerators have been utilized over the last twenty years in measurements of the cross sections for scattering to excited nuclear states. From such studies we have gained much of our present knowledge about the properties of the response of the nucleus to electromagnetic excitation and, in consequence, much of what we know about nuclear dynamics in general.

This first generation of machines is now being replaced with new combinations of accelerators and analysis systems which are characterized both by significantly higher beam energies and greatly improved energy resolution in the detected spectra of scattered electrons. These new facilities have the potential to produce data which have the range of momentum transfer, the precision of final state specification and the statistical accuracy to fully test the detailed predictions of modern nuclear theories about the electromagnetic excitation of nuclei. In this review we summarize and evaluate the existing experimental information in one area of inelastic electron scattering studies, the electric quadrupole and hexadecupole excitations of light, even-A nuclei. We carry out this review in the context of the predictions of the "neo-classical" shell-model theory of nuclear structure. We attempt to illustrate the level of theoretical understanding of these electric excitations which has been reached with the aid of current experimental knowledge and the potential increases in understanding which better resolution data from higher energy beams could provide.

Historically, most of the data we consider here were originally compared with predictions of one or another of the collective models of nuclear structure and nuclear excitations (Ref 11, Ref 12). These models postulate general functional forms of the transition charge densities from which the electron scattering cross sections are calculated. The parameters of these functions are conventionally fixed by adjusting them to best reproduce the data at hand. These collective-model analyses have been valuable in qualitatively characterizing the nature of the excitations and in condensing the data into concise parametrizations. However, the results of such analyses are not easily linked to other features of nuclear structure.

To achieve a theoretical integration of the results of inelastic electron scattering studies into the wider arena of nuclear structure it is necessary to analyze the scattering data with a microscopic theory which accounts for such diverse aspects as nucleon transfer, beta decay, static electromagnetic moments and non-collective inelastic excitations on an equal footing with the collective excitations which dominate the electron scattering spectra. In order to move beyond local phnomenalogical parametrizations it is also important to establish whether or not the changes in the features of the electron scattering data which are observed as the target nuclei are varied can be understood in terms of some underlying general theory of nuclear structure. In a complementary sense, of course, the capability of

explaining such unambiguous and fundamental results as those embodied in inelastic electron scattering data are a primary criterion by which the success of such a comprehensive microscopic theory of nuclear structure should be evaluated.

We study in this review the predictions for E2 and E4 inelastic electron scattering which are obtained from a formulation of the classical nuclear shell model. The theoretical wave functions we use to calculate the transition charge densities for 0+ to 2+ and 4+ inelastic scattering transitions are obtained in calculations (Ref 13) which generalize the classical nuclear shell model of Mayer and Jensen (Ref 14) to consider the complete mixing of the shell-model configurations which are included between the magic numbers of 16 and 40. This approach to understanding nuclear structure is not oriented towards explanation of the type of collective electric quadrupole excitation phenomena which inelastic electron scattering cross sections emphasise. It focusses, rather, on explanations of the spectra of energy levels and the single-nucleon constitutions of these levels. Nonetheless, some collective features of the energy level structures can emerge from the configuration mixing which is implicit in the theory. Comparison of the predictions of these features with the results of inelastic electron scattering experiments provides the most thorough and illuminating test possible of whether this theoretical approach yields a relatively complete and internally consistent understanding of nuclear structure.

I.1. Inelastic electron scattering and electric multipole transitions

We are concerned in this study with the relationship between model wave functions for nuclear states and form factors for electron scattering, specifically with shell-model wave functions for sd-shell nuclei and longitudinal-electric E2 and E4 form factors for 0+ to 2+ and 0+ to 4+ transitions, in conjunction with the associated elastic scattering. We wish to establish how well the shell-model formulation, together with its necessary auxiliary theoretical appurtenances, can quantitatively reproduce these experimental results. In making comparisons between experimental and theoretical form factors we also wish to distinguish as clearly as possible the effects of the shell-model predictions of configuration mixing from the effects of how the radial profiles of the single-nucleon wave functions are specified and of how the contributions of extra-model-space excitations are introduced into the calculations.

Knowledge of electric quadrupole matrix elements between nuclear states is fundamental to our understanding of nuclear structure. Measurements of the longitudinal components of electric quadrupole (e,e') transitions can significantly augment, both in quantitative and qualitative terms, the E2 data which are available from measurements of gamma-ray transitions. The scattering process in principle allows

the study of transitions from the ground state to all excited states within the boundaries of the E2 selection rules. Thus, the only limitations to experimental observations in (e,e') are the practical ones of counting statistics and energy resolution. This is in contrast to the situation in gamma-ray decay, where many unavoidable lacunae result from lifetimes, branching ratios and mixing ratios which are unmeasurable with current techniques and from the instability with respect to nucleon decay of higher excited states. Much more important than this simple quantitative augmentation of our knowledge of E2 phenomena, however, is the qualitatively new dimension which stems from the measurement of the transition probabilities at a variety of momentum transfers. From the relationship between momentum and position these measurements yield information on the radial distribution of the transition process. Thus, a longitudinal E2 form factor yields the "transition strength as function of radius" rather than just the "integral" of this function which is obtained from a measurement of B(E2).

Study of electric hexadecupole phenomena is a logical extension of electric quadrupole studies to more detailed aspects of shape-collective nuclear phenomena. Progress on this topic in light nuclei is totally dependent on scattering experiments because all E4 decay branches are, in practice, unmeasurably small with respect to the competing E2 branches. As with E2 scattering, the longitudinal E4 form factors yield not only an estimate of the B(E4) but also information about the radial structure of the underlying transition density.

While it is convenient and conventional to treat the information contained in form-factor data as subsuming the information contained in the corresponding measuremants of B(E2) in gamma-ray transition experiments, such is not exactly the case. Form-factor measurements cannot in practice be extended in to the momentum transfer of the "photon point", $q = E_f - E_i$, the energy difference between the two nuclear states, and the extraction of B(EL) from the form-factor data thus requires a model-dependent extrapolation from the range of measurement into the photon point. We investigate in this study typical uncertainties in such extrapolations and compare, where both exist, direct measurements of B(E2) with the (e,e') data.

Elastic and inelastic E2 and E4 electron scattering data from the sd-shell have been compared previously (Ref 15, Ref 16, Ref 17, Ref 18, Ref 19.) with form factors calculated from wave functions(Ref 20, Ref 21)which are genetic ancestors of those employed here. The general outlines of the results of the present more extensive and detailed study are consistent with the results of this earlier work but the conclusions and inferences drawn here from these results will be seen to differ in some respects from those of Ref 16 and Ref 18.

I.2. Foundations of the nuclear-structure model

The conventional multiparticle, configuration-mixing, shell model employed in this study deals explicitly only with the distributions and coupling of the "valence" (relative to some inert core) nucleons within a few "model-space" orbitals. The present study of the even-mass stable nuclei from ^{20}Ne through ^{36}Ar is based on the usual shell-model approximation for this region in which excitations across the ^{16}O or ^{40}Ca shell closures are forbidden. The only active orbits of the model are thus those labeled by the quantum numbers nlj = $0d_{5/2}$, $1s_{1/2}$ and $0d_{3/2}$. Our assumption is hence that the A nucleons of an "sd-shell" state in an $8<N,Z<20$ nucleus are apportioned such that 8 neutrons and 8 protons are held inert in the $(0s_{1/2}^4 \quad 0p_{3/2}^8 \cdot 0p_{1/2}^4 \quad)_{J=0,T=0}$ configuration and the remaining A-16 nucleons distributed over all possible combinations of the $0d_{5/2}$, $1s_{1/2}$ and $0d_{3/2}$ orbitals. We use the complete sets of $sd^{(A-16)}$ basis states for the expansions of the model wave functions for the states of each A value, so that the results for the different nuclei are all treated uniformly with respect to the sd-shell space and no allowance need be made for relative truncations from mass to mass of the sd-shell configurations themselves.

The wave functions we use for each A value are obtained from diagonalization of a new empirical Hamiltonian (Ref 22)designed for complete-space sd^n calculations throughout the A = 17-39 region. This new Hamiltonian produces correspondences between model expectation values and experimental measurements which, upon

preliminary inspection, are clearly superior in the aggregate to those from any previous formulation or set of formulations for this region. Of course, it does not follow that wave functions from the new Hamiltonian for specific states are necessarily always superior to those available from other formulations. However, for a systematic study across the entire shell the present wave functions are, by construction, preferable to any extant alternative. The values assumed for the one and two-body matrix elements of shell-model Hamiltonian govern the distribution of the wave-function amplitudes over the various basis states of the $sd^{(A-16)}$ systems and the determination of these amplitudes via diagonalization constitutes the solution of the classical shell-model problem.

Prescriptions for the radial components of the wave functions of the single-nucleon states of the shell-model space do not explicitly emerge as part of this classical shell-model solution. Rather, these aspects of the complete specification of nuclear states are grafted onto the shell-model amplitudes ex post facto via independent assumptions about the form of the mean field from which the shell-model orbitals are generated. Knowledge of the radial characteristics of the single-nucleon wave functions is not vital for the calculation of some nuclear observables, such as magnetic dipole moments and Gamow-Teller beta decay. Even for calculations of B(E2) values, detailed accuracy is not important beyond qualitative reproduction of the correct rms radii of the states. However, when the objects of study are themselves functions of radius, as is the case

with (e,e') form factors, attention obviously must be paid to how the single-nucleon wave functions are generated and to the effects of different prescriptions for their generation upon the calculated form factors. We investigate here three conventional models for the single-nucleon potential and the effects of different parametrizations of these models. Even so, we are at pains to disclaim having treated this aspect of the total form-factor problem exhaustively. Rather, we aim at illustrating from our studies of these simple examples the range within which different choices of the radial profiles of the single-nucleon wave functions can alter the predicted form factors.

Shell-model wave functions cannot properly reproduce measured nuclear properties exactly if the active model nucleons are assumed to have the same properties as those of neutrons and protons in free space. Most simply, this is merely a consequence of the impossibility of having an exact overlap between model wave functions, from which excitations from the core into the model-space or higher orbits, or out of the model-space orbits into higher orbits, are totally excluded, with the real, "physical", nuclear states, in which such excitations obviously occur to some degree. The values of some observables, such as magnetic-dipole moments and transition rates for example, are relatively insensitive to such differences between physical and model wave functions because the selection rules for the transition operator inhibit connections between the "intra-model-space" and "extra-model-space" components of the physical states. The values of other observables, however, such as

electric-quadrupole moments and transition rates, for example, are quite sensitive to the extra-model-space components of the physical states. For such phenomena, an additional ingredient must be added to the classical nuclear shell model in order to achieve absolute, as opposed to relative, agreement between theory and experiment.

The conventional approach to supplying this added ingredient to shell-model wave functions is to redefine the properties of the valence nucleons from those exhibited by actual neutrons and protons in free space to model-effective values. The implicit assumption of this approach is that the contributions of the extra-model-space components of the physical wave functions to the observed matrix elements are proportional to the intra-model-space matrix elements. The detailed variations in transition strengths which are observed to occur from state to state are thus assumed to result completely from differences in the shell-model eigenfunctions rather than from any state-dependent interplay between the model-space and extra-model-space components of the "real" wave functions. In this assumption, the effects of the existence of extra-model-space components in the physical wave function and of their mixing with the intra-model-space components are introduced into the model as state-independent renormalizations of the operators upon the model wave functions which describe the various observables of nuclear spectroscopy.

For electric quadrupole and hexadecupole phenomena, these

renormalizations (the "core-polarization" corrections) which compensate for the important components of the "real" states which are missing in the model wave functions (presumably these are fractions of the L-$\hbar\omega$ EL "giant resonances") are conventionally accomplished by giving the neutron and proton "effective" charges. In its usual form, this "effective charge" model amounts to evaluating the matrix elements of the electric multipole operators between the model-space wave functions under the assumption that model neutrons and protons have charges e_n and e_p different from, respectively, 0 and 1e. It is implicit in this procedure that the extra-model-space component of the transition has the same radial dependence as the intra-model-space component. However, if the extra-model-space component has its origins in a phenomena such as mixing of the model wave function with the giant resonance, its radial dependence might be different from that of the model-space component itself. This question of radial form cannot be addressed directly with B(E2) values alone. In the study of (e,e') phenomena however, the radial dependence of both components affect the calculated form factors. The choice of a model for the "effective charge" contribution is thus an important ingredient of the complete shell-model-based theory for longitudinal-electric (e,e') data. Comparison of the data with calculated form factors based on different core-polarization models of the effective-charge type may point toward a preferred choice for this component of the theory.

I.3. Summary

Our goal in this study is to delimit what may be expected from attempts to calculate longitudinal-electric form factors from conventional, few-orbit shell-model wave functions. We use shell-model wave functions from a comprehensive calculation for the entire sd shell to calculate the matrix elements of the sd-shell one-body transition density for the 0+ to 2+ and 0+ to 4+ transitions in the even-mass nuclei from A = 20 through 36 and the occupation probabilities of the ground states. Single-nucleon wave functions generated according to several different prescriptions are then combined with these matrix elements for the one-body transitions between the multiparticle shell-model states to create "model-space" transition densities. These model-space transition densities are then, in turn, combined with each of two alternate models for the radial distribution of the "extra-model-space", core-polarization transition density to form "total" transition densities. Finally, these total transition densities are used in plane-wave or distorted-wave Born approximation calculations for the electron-scattering process. The resulting form factors, corrected for finite-nucleon-size and center-of-mass effects, are then compared with experimental data. We wish to know if one or the other of the models for the core-polarization transition density can be identified as preferable and which, if any, of the prescriptions for single-nucleon radial wave functions seems best. We wish to determine if the uncertainties in the

proper prescription of these auxiliary components of shell-model form factors are small enough to permit a critique of the details of the shell-model wave functions themselves and, finally, if this is possible, what the results of such a critique are.

II. Theoretical formulation

II.1. Introduction

The general theory for electron scattering from nuclei is given in many sources, for examples, in Ref 23, Ref 3, Ref 24 and Ref 25. The cross section for the scattering of an electron from a nucleus of mass M and charge Z in the one-photon-exchange approximation is (with $\hbar = c = 1$)

$$d\sigma/d\Omega = (d\sigma/d\Omega)_{Mott} \quad (1/\epsilon) \sum_L \{ (q_\mu^2/q^2)^2 F^2_{LE,L}(q) + (\frac{q_\mu^2}{2q^2} + \tan^2\theta/2) \ [F^2_{TE,L}(q) + F^2_{TM,L}(q)]\}$$

where $$\epsilon = 1 + (2E_{e,i}/M) \sin^2(\theta/2). \qquad (1)$$

In this equation $d\sigma/d\Omega$ is the differential cross section for the scattering of an electron into the solid angle $d\Omega$ at the laboratory angle Θ and ϵ is the nuclear-recoil factor. The four-vector momentum transfer q_μ and the vector momentum transfer q are given by

$$q_\mu^2 = q^2 - (E_{e,i} - E_{e,f})^2 \qquad (2)$$

and

$$q^2 = 4 E_{e,i} E_{e,f} \sin^2(\theta/2) + (E_{e,i} - E_{e,f})^2 \qquad (3)$$

$E_{e,i}$ and $E_{e,f}$ are the total energies of the incident and scattered

electrons respectively.

In conventional units the momentum transfer contains the factor $(\hbar c)^{-1}$ and will be given in our work in units of fm^{-1}. The Mott cross section for relativistic electron scattering from a point charge (neglecting the rest mass of the electron) is given by

$$(d\sigma/d\Omega)_{Mott} = \frac{Z^2\alpha^2 \cos^2(\theta/2)}{4E_{e,i}^2 \sin^4(\theta/2)} \qquad (4)$$

where Z is the charge of the target nucleus and α is the fine-structure constant.

The quantities F_{LE}, F_{TE} and F_{TM} are, respectively, the longitudinal-electric (or "Coulomb"), transverse-electric and transverse-magnetic nuclear form factors. In this work we are concerned with elastic scattering from spin-zero nuclei and inelastic excitations from 0+ to 2+ and 4+ states measured at forward angles. It is conventional in these cases to divide out the kinematic factors in Eq.(1) so as to obtain experimental "LE" form factors directly. In the following discussion we will refer to either F_{LE} or F^{λ}_{LE} as the "form factor". The subcript "LE" will be dropped and the subscript "ch", "p" or "n" will be added for the convenience of distinguishing the "charge" form factors, which correspond to observed electron scattering, from the "point"-proton and "point"-neutron form factors which emerge from the nuclear structure calculations before corrections are made for finite-nucleon-size and center-of-mass effects.

In the plane-wave Born approximation (PWBA) the form factor is given by the Fourier-Bessel transform of the nuclear transition density $\rho(r)$. This transition density for point protons or neutrons (τ_3 = +/-1 = p/n) can be expressed as

$$\rho_{L,\tau_3}(r) = \langle f \| \rho^{op}_{L,\tau_3}(r) \| i \rangle \qquad (5)$$

where

$$\rho^{op}_{L,\tau_3}(r) = \sum_k^{\tau_3} r_k^{-2} \delta(r - r_k) Y^{(L)}(\Omega_k) \qquad (6)$$

The τ_3 over the summation indicates that the sum over nucleons is restricted to either protons or neutrons. Our reduced matrix element convention is that of Edmonds (Eq.5.4.1) (Ref 26). The normalized PWBA form factor is given by

$$F_{L,\tau_3}(q) = N_{F,\tau_3} \, 4\pi \int j_L(qr) \rho_{L,\tau_3}(r) r^2 dr \; G_{CM}(q) \qquad (7)$$

where the normalization constant N_F is chosen so that the elastic (L=0) form factors are unity at q=0:

$$N_{F,p} = Z^{-1}[4\pi/(2J_i+1)]^{\frac{1}{2}} \qquad (8)$$

$$N_{F,n} = N^{-1}[4\pi/(2J_i+1)]^{\frac{1}{2}} \qquad (9)$$

The numbers of protons and neutrons in the nucleus are denoted, respectively, by Z and N. The transition densities are conventionally calculated relative to the center of mass of the single-nucleon

potential. Thus in Eq.(7) we include the center-of-mass correction factor G_{CM} given by the harmonic-oscillator approximation (Ref 27)

$$G_{CM}(q) = \exp(q^2 b^2 / 4A) \qquad (10)$$

where A = N + Z and where b is the oscillator length parameter obtained from the ground-state rms charge radii (Ref 28). Transition densities which include the center-of-mass correction can be obtained from the inverse Fourier-Bessel transformation of Eq.(7).

The longitudinal-electric charge form factors for electron scattering are obtained from those of the point-nucleon approximation by multiplying the latter by the respective free-nucleon form factors $G_{fs}(q)$ which take into account the nucleon finite size:

$$F_{L,ch}(q) = F_{L,p}(q) \, G_{fs,p}(q) + (N/Z) \, F_{L,n}(q) \, G_{fs,n}(q) \qquad (11)$$

Except for the more precisely measured elastic form factors, it is an adequate approximation to use the simpler form of Eq. (11):

$$F_{L,ch}(q) = F_{L,p}(q) \{ G_{fs,p}(q) + (N/Z) \, G_{fs,n}(q) \} \text{ for } L>0 \qquad (12)$$

We use the nucleon form factors from Ref 29 which give mean-square charge radii of 0.774 fm^2 and -0.116 fm^2 for the proton and neutron, respectively. In addition, we include the small Darwin-Foldy relativistic correction in G_{fs} (Ref 2). The

relativistic spin-orbit correction (Ref 2, Ref 30) is small and has not been included.

In our calculations the total transition density is constructed as the sum of two contributions. One, the "model-space" component, originates within, and is confined to, the active shell-model space, the sd shell in the present calculations. We will denote this component with the symbol A(r). The other, the "extra-model-space" or "core-polarization" component, can involve all configurations. We will denote it by C(r). In terms of these two components the total transition density is given by

$$\rho(r) = N_A A(r) + N_C C(r) \qquad (13)$$

Our notation for the r^L integrals of these radial functions will be:

$$M_L = 4\pi \int r^L \rho(r)\, r^2 dr \qquad (14)$$

$$A_L = 4\pi \int r^L A(r)\, r^2 dr \qquad (15)$$

$$C_L = 4\pi \int r^L C(r)\, r^2 dr \qquad (16)$$

These definitions for the matrix elements A and M are those used in Ref 31.

In Section II.2 the details of the calculations for the sd-shell model-space transition densities are presented. Models for the single-nucleon radial wave functions are discussed in Section II.3.

Models for the core-polarization transition densities and the normalization constants N in Eq.(13) are discussed in Section II.4. In Section II.5 the differences between PWBA calculations for the scattering process and the more realistic, but also more complex, DWBA calculations are noted. Finally, a representation of the form factors which provides a convenient display of results from both form-factor and gamma-ray-transition data is derived in Section II.6.

II.2. Model-space transition densities.

The model space for the present calculations consists of the complete set of states spanned by the orbits $0d_{5/2}$, $1s_{1/2}$ and $0d_{3/2}$. The eigenstates corresponding to the levels of concern in A=20-36 nuclei were obtained from diagonalizations of the "universal sd" (USD) interaction of Wildenthal (Ref 22). Matrix elements between these multiparticle model states of a one-body tensor operator $O^{(L)}$ are conveniently expressed as a sum over elements of the one-body density matrix (OBDM) and the corresponding elements of the single-nucleon transition density (SNTD)

$$\langle (sd)^n, f \| O^{(L)}(\tau_3) \| (sd)^n, i \rangle = \sum_{j,j'} \mathrm{OBDM}(i,f,L,j,j',\tau_3)\,\mathrm{SNTD}(O,L,j,j',\tau_3) \qquad (17)$$

where

$$OBDM(i,f,L,j,j',\tau_3) = (2L+1)^{-\frac{1}{2}} \times$$
$$\langle (sd)^n, f \| [a^\dagger(j,\tau_3) \otimes \tilde{a}(j',\tau_3)]^{(L)} \| (sd)^n, i \rangle \qquad (18)$$

and

$$SNTD(O,L,j,j',\tau_3) = \langle j,\tau_3 \| O^{(L)} \| j',\tau_3 \rangle \qquad (19)$$

The j,j' sums extend over the three sd-shell orbits in the case of inelastic transitions. For the elastic $L = \emptyset$ matrix elements the orbits in the ^{16}O core are also included in the sum. We abbreviate the entire set of quantum numbers (n,l,j) by (j) and the specifications of the initial and final states ($A_{i/f}$, $Z_{i/f}$, $v_{i/f}$, $J_{i/f}$, $T_{i/f}$) by (i/f) in these equations. The operator $a^\dagger(j,\tau_3)$ creates a neutron or proton in the single-nucleon state j and the operator $\tilde{a}(j',\tau_3)$ annihilates a neutron or proton in single-nucleon state j'.

The single-nucleon transition-density operator corresponding to Eq. (6) is given by

$$SNTD(j,j',\rho^{OP}) = R(j,\tau_3,r)R(j',\tau_3,r)\langle j \| Y^{(L)} \| j' \rangle \qquad (2\emptyset)$$

The radial wave functions R will be described in Sec. II.3. The sd-shell transition density is then given by

$$A_{L,\tau_3}(r) = \sum_{j,j'} OBDM(i,f,L,j,j',\tau_3) SNTD(j,j',\rho^{OP}) \qquad (21)$$

The sd-shell wave functions generated with the USD interaction have good isospin and it is convenient to calculate the OBDM in terms of isospin-reduced matrix elements. The relation between these "triply reduced" OBDM and the p/n OBDM of Eq. (18) is

$$OBDM(p/n) = (-1)^{T_f - T_z} \sqrt{2} \begin{pmatrix} T_f & \emptyset & T_i \\ -T_z & \emptyset & T_z \end{pmatrix} OBDM(\Delta T = \emptyset)/2$$
$$(+/-)(-1)^{T_f - T_z} \sqrt{6} \begin{pmatrix} T_f & 1 & T_i \\ -T_z & \emptyset & T_z \end{pmatrix} OBDM(\Delta T = 1)/2 \qquad (22)$$

where OBDM(ΔT) is given by

$$OBDM(i,f,L,\Delta T,j,j') = (2\Delta T+1)^{-\frac{1}{2}}(2L+1)^{-\frac{1}{2}} \times$$
$$\langle (sd)^n, f \| [a^\dagger(j) \otimes \tilde{a}(j')]^{(L,\Delta T)} \| (sd)^n, i \rangle \qquad (23)$$

The OBDM (ΔT) contain all of the information about transitions of given multipolarities which is embedded in the model wave functions. The values which are used in the calculations of the form factors presented in this work are presented, along with the calculated excitation energies and the measured excitation energies of the observed levels to which the model states are presumed to correspond, in Tables (1), (2) and (3)

II.3. Radial components of single-nucleon wave functions

The shape of the model-space transition density A of Eq. (21) depends upon the detailed form of the radial components $R(j, \tau_3, r)$ of the single-nucleon wave functions of Eq. (20). For the present study we have used eigenfunctions of several standard models for the single-nucleon potential as explicit representations of these radial wave functions. We use the harmonic-oscillator (HO) potential in many calculations. We use the parameter b ($b^2 = 41.65/\hbar\omega$) to define the radial scale of this one-parameter, infinite-depth potential model and employ one or the other of two prescriptions to assign its value for a given form-factor calculation.

For each of the transitions we consider in this study we will show a form factor which incorporates a model-space transition density A(r) based on single-nucleon wave functions of an HO potential whose b-value ($b=b_{rms}$) is set so that the measured rms radius of the ground state in question is reproduced by a simple model (Ref 28). This model assumes the wave functions of all occupied and partially occupied orbits are generated from a single potential parametrization and that this potential has the harmonic-oscillator form. The pertinent rms radii and the corresponding values of b_{rms} (Ref 28) are listed in Table (4). (The primacy of the ground state over an excited state in choosing a radial normalization merely reflects the lack of a practical alternative. Since the radii of different states in a given nucleus may well differ it seems

appropriate to explicitly note that this implicit choice constitutes yet another of the many assumptions which must be made in calculating "the" theoretical form factor.) Alternatively, in some special cases we also show form factors obtained by using values of b ($b=b_{fit}$) which optimize the agreement between calculated and measured E2 form factors rather than the b-values which reproduce the ground-state rms radius.

We will also show form factors based on model-space transition densities which incorporate single-nucleon wave functions from finite-depth potential models. For the general case in which these potentials can be non-local, the radial wave functions R(j,r) are obtained from the set of equations (Ref 32)

$$\left[\frac{-\hbar^2}{2\mu}\frac{d^2}{dr^2} + \frac{\hbar^2 \ell(\ell+1)}{2\mu r^2} + U_{local}(r)\right] \psi_{local}(r) = \varepsilon\, \psi_{local}(r) \tag{24}$$

where

$$R(j,r) = [\, m^*(r)/m \,]^{1/2} \; \psi_{local}(r) \tag{25}$$

and

$$U_{local}(r) = [\, 1 - m^*(r)/m \,]\,\varepsilon \;\; + [\, m^*(r)/m \,]\, U(r) \tag{26}$$

The potential U(r) is divided in the usual way into central, spin-orbit and Coulomb components,

$$U(r) = V(r) + V_{SO}(r)\, \langle \vec{l}\cdot\vec{\sigma} \rangle + \delta_{pn} V_{Coulomb}(r) \tag{27}$$

where δ_{pn} is equal to 1 for protons and 0 for neutrons.

We will consider two models for the central potential V(r), the Woods-Saxon parameterization $V_W(r)$ and a Skyrme-Hartree-Fock potential $V_S(r)$. They are expressed as

$$V_w(r) = V(\tau_3)[\ 1 + \exp(r-R(\tau_3))/a(\tau_3)\ ]^{-1} \qquad (28)$$

and

$$V_S(r) = F\ [\rho_{0,p}\ (r), \rho_{0,n}\ (r)\ ] \qquad (29)$$

In the Woods-Saxon potential, $V(\tau_3)$, $R(\tau_3)$ and $a(\tau_3)$ are the constants for the well depth, radius and diffuseness. The Skyrme functionals F of the proton and neutron densities (Eq. 5) are given by Dover and Van Giai (Ref 32) as the quantity inside the first square bracket in their Eq.2.12. [Note that in their Eq.2.5 the term $(1/2)(t_1 + t_2)$ should be replaced by $(1/4)(t_1 + t_2)$.]

Standard forms are used for the Coulomb and spin-orbit terms in Eq.(27). In the Woods-Saxon calculations we use a Coulomb potential based on a uniform-charge-density distribution which has total charge number Z-1 and the experimental rms charge radius and a spin-orbit potential based on the usual derivative of a Fermi shape which has strength $(\hbar/m_\pi c)^2$ Vso = 12 MeV, radius 1.1 $A^{1/3}$ fm and diffuseness 0.65 fm. In the Skyrme-Hartree-Fock calculations we use a Coulomb potential calculated by folding the Coulomb interaction with the calculated charge density ρ_{ch} (r) plus the approximation for the exchange term given by Beiner et al. (Ref 33) and the

spin-orbit potential given by the first term on the right-hand side of Eq.2.6 of Ref 32. The effective mass m*(r)/m is given in terms of the nucleon densities and the Skyrme parameters by Eq.(2.3) of Ref 32 or Eq.(33) of Ref 34. For the Woods-Saxon calculations we use the conventional reduced mass $\mu = m(\tau_3)\ (A-1)/A$ and for the Skyrme-Hartree-Fock calculations a reduced mass which includes a center-of-mass correction for the total energy (Ref 35), $\mu = m(\tau_3)\ A/(A-1)$.

The three parameters of the Woods-Saxon potentials we use here were obtained for each mass-number A via interpolations between the values obtained for ^{16}O and ^{40}Ca. The parameters for each of these two cases were uniquely obtained by requiring an exact match between calculated and measured values of the r^2 and r^4 moments of the charge distribution and of the binding energy of one valence orbit. Details of these fits and the resulting parameters are given in Ref 34, as is the dependence of the results upon the effective mass. The calculations presented here were obtained with the "local" [m*(r)/m=1] potential. Calculations for the form factors which utilized the "non-local" potential of Ref 34 were not significantly different from those with the "local" potential and we do not present them here.

We have investigated the consequences for form factors of single-nucleon wave functions generated by potentials obtained from Hartree-Fock calculations (Ref 36) which employ Skyrme

interactions of which the Skyrme III interaction of Ref 33 is typical. Even though the rms radii obtained with single-nucleon wave functions from this potential are in reasonable agreement with experiment (see Table 4), the corresponding elastic form factors will be seen not to agree with experiment at the higher momentum transfers as well as do the form factors obtained with the oscillator and Woods-Saxon potential models, particularly for ^{24}Mg and ^{28}Si. The inelastic form factors calculated with these Skyrme-Hartree-Fock radial wave functions do not give any significant improvement over those obtained with the Woods-Saxon wave functions and therefore will not be presented.

II.4. Core-polarization transition densities.

It is well known, as mentioned above, that model-space matrix elements with "free-nucleon" normalizations do not adequately describe the absolute magnitudes of observed E2 gamma-ray-transition probabilities, presumably because of the polarization in nature of the core protons by the model-space protons and neutrons. It has been empirically established (Ref 37, Ref 34) that the introduction of state- and mass-independent "effective charges" for the model-space protons and neutrons are adequate to obtain systematic quantitative agreement between experiment and shell-model predictions for B(E2) values in the sd-shell. The justifications for this

empirical procedure can be qualitatively understood from a first-order perturbation theory calculation of the OBDM for the $2\hbar\omega$ 1p-1h transitions not included in the model space (Ref 38, Ref 39). A quantitative calculation is much more difficult since it depends upon the poorly understood effective interactions in finite nuclei as well as upon the higher-order contributions. Therefore, at this stage we will rely on simple empirical models to extend the effective-charge concept for the gamma-ray-transition matrix elements to the transition densities which are needed to describe the scattering data.

The most economical model for the core-polarization transition density is to make it exactly proportional to the model-space transition density. We will refer to this as the "valence" (V) model.

$$C^{V}_{L,\tau_3}(r) = A_{L,\tau_3}(r) \qquad (30)$$

A somewhat more sophisticated model has its motivation from first-order perturbation calculations with the schematic multipole-multipole interaction $[r_1^L Y_1(L)]\cdot[r_2^L Y_2(L)]$. This interaction can only connect the ground state to the L-multipole $n\hbar\omega$ giant resonances. The shape of the transition densities for these excitations is given by the Tassie (T) model (Ref 11) for L>1, and we assume this shape for the second of the two models for the core-polarization transition density which we investigate here.

$$C^{T}_{L,\tau_3}(r) = r^{L-1} d\,A_{0,\tau_3}(r)/dr \qquad (31)$$

where A(r) is the ground-state density, commonly expressed as

$$\rho_{gs,\tau_3}(r) = A_{0,\tau_3}(r)/(4\pi)^{\frac{1}{2}} \qquad (32)$$

Empirical charge-density distributions have been deduced for ^{24}Mg, ^{28}Si and ^{32}S by Li et al. (Ref 40) from their elastic scattering data on these nuclei. We have used their results for ^{28}Si and ^{32}S as the densities in Eq. (32). (Since the nucleon-finite-size and center-of-mass corrections are made at a later stage in our calculations, at this stage we unfold these corrections from these empirical charge densities.) However, the parameterizations by Li et al. of these ground state densities are not constrained to yield non-negative values of the densities. We find that while for Si and S the negative-density regions (which occur at large values of r) are very small in magnitude, that for Mg is non-negligible, particularly when weighted by the high power of r attendant to calculation of E4 form-factors. As a consequence, use of the empirical density for Mg in the generation of the Tassie core-polarization transition density from Eq. (32) gives rise to anomalies at low q values. Hence, in the cases of ^{24}Mg and the sd-shell nuclei for which the elastic scattering data are sparse, we use ground-state densities calculated from the models assumed for the single-nucleon wave functions and the shell-model occupation probabilities of Table (3).

Only the radial shapes of the core-polarization transition densities are described by Eqs. (30) and (31). The normalization

factors in Eq.(13) are obtained from the $q = E_i - E_f$ gamma-ray-transition matrix elements expressed in terms of the effective charges (Ref. 39):

$$M_p = A_p (1 + \delta_{pp}) + A_n \delta_{pn} \qquad (33)$$

$$M_n = A_n (1 + \delta_{nn}) + A_p \delta_{np} \qquad (34)$$

where δ_{cv} is the polarization charge due to the interaction of the valence nucleons (v) with the core nucleons (c). For the sd-shell nuclei, with their approximately equal numbers of neutrons and protons, it is a good approximation to set $\delta_{nn} = \delta_{pp}$ and $\delta_{pn} = \delta_{np}$. The remaining two parameters are related to the conventional effective-charge parameters e_p and e_n by

$$\delta_{pp} = \delta_{nn} = e_p - 1 \qquad (35)$$

$$\delta_{pn} = \delta_{np} = e_n \qquad (36)$$

We will use the effective-charge values of $e_p + e_n = 1.7e$ for E2 and $e_p + e_n = 2.0e$ for E4 which are suggested by surveys of sd-shell data in the context of antecedant shell-model wave functions (Ref 37, Ref 31) and, alternatively, some other E2 effective-charge values suggested by individual form factors. In all cases we will use an isovector effective charge defined by $e_p - e_n = 1e$ (Ref 34).

We will assume that N_A is unity. Then, the normalization constants N_c in Eq. (13) are obtained by comparing the integrals of both sides of this equation to Eqs. (33) and (34) to obtain the results:

$$N_{A,p} = N_{A,n} = 1 \tag{37}$$

$$N_{C,p} = (\delta_{pp} A_p + \delta_{pn} A_n)/C_p \tag{38}$$

$$N_{C,n} = (\delta_{nn} A_n + \delta_{np} A_p)/C_n \tag{39}$$

The fact that N_A is unity is related to the first-order pertubation-theory approximation. In higher order there are additional contributions to the core-polarization transition density as well as renormalization terms which reduce the N_A from unity. These two contributions tend to cancel each other and the choice $N_A = 1$ may still be appropriate if the radial shape of the higher-order contributions is similar to the model-space transition density.

To provide a touchstone for comparisons with our microscopic calculations discussed below, we compare in Fig. (1) the E2 and E4 form factors obtained from the pure Tassie-model transition densities (dashed lines) with the experimental data for ^{28}Si. (The relationship between the M(q) and F(q) is given in Section II.6.) In addition, we show in Fig. (1) the form factors obtained from the transition densities (solid lines)given by the model of Bohr and Mottelson (Ref 41, p.343), who consider deformations that distort the radius parameter while leaving the surface diffuseness independent of angle:

$$C^{BM}_{L,T_3}(r) = d\,A_{0,\tau_3}(r)/dr \tag{40}$$

The theoretical curves shown in Fig. (1) have been arbitrarily normalized to give the same B(EL) values. The shape of the

Bohr-Mottelson form factor is clearly in good agreement with experiment and shows the success of this model in describing the low-lying collective states even in light nuclei. One of the goals of our calculations and comparisons is to determine the extent to which shell-model calculations within the confines of a single major shell are able to describe this collective feature and at the same predict the relative strengths and shapes for the variety of other collective and single-particle degrees of freedom manifested in the nuclei of this region.

II.5. Differences between PWBA and DWBA calculations

The inelastic-scattering form factors we present in this study are calculated in the plane-wave Born approximation (PWBA). It is thus necessary to determine the extent to which distortion effects might be the source of any observed differences between the calculations and experiment. The zeroth-order distortion correction is obtained by using an "effective" momentum transfer q_{eff} in place of q (Ref 3)

$$q_{eff} = q\left[1 + \frac{3Ze^2}{2E_e R_{ch}}\right] \tag{41}$$

where R_{ch} is related to the rms charge radius, r_{ch}, by $R_{ch} = \sqrt{5/3}\, r_{ch}$. Thus we plot the PWBA calculations vs. q, while the experimental data and the DWBA calculations are plotted vs. q_{eff}. Since the finite-

size and center-of-mass corrections are applied to the form factor rather than to the transition density, q_{eff} is used in place of q for these corrections in the DWBA calculations and, in addition, we use $D_L(q_{eff})$ in Eq. (50) below in such cases.

We have carried out distorted-wave Born approximation (DWBA) calculations with the MIT elastic phase-shift code (Ref 42) and the DUELS inelastic code (Ref 43). In Fig. (2) we show examples of comparisons between the PWBA (dashed lines) and DWBA calculations (solid lines) for scattering on ^{28}Si. (The M(q) vs. q representations of the E2 and E4 form factors are explained in Section II.6.) For the elastic form factor, the DWBA corrections to PWBA are obviously important in order to obtain quantitative agreement with the precise experimental which are available ;Hence, we will compare elastic scattering data with DWBA calculations in evaluating the various components of the theory, in accord with the conclusions of Ref 17.On the other hand, we see from Fig. (2) that for inelastic form factors, the DWBA results do not differ significantly from the PWBA shapes except in that the first minimum at finite q in the E2 form factor is filled in by the DWBA corrections. In view of the limited precision of the inelastic data and the limited accuracy of the theoretical fits to these data, we conclude that at the masses and energies relevant to the present study there is no significant advantage to replacing PWBA calculations for inelastic scattering with the lengthier and more complex DWBA calculations, in contrast to the implications of Ref 16. We thus will use PWBA calculations in our

studies of inelastic form factors, while remembering the small systematic ways in which they differ from the corresponding DWBA results.

II.6. Conversion of form factors to q-dependent matrix elements M(q)

The conventional displays of form factors, in which F(q) or $F(q)^2$ is plotted against q (see Fig. (2)), do not allow a simultaneous display of the B(E2) value obtained from measurements of gamma-ray transition strengths with the scattering data. In addition, the exponential-type dependences of F(q) upon q dictate logarithmic display scales which tend to submerge details. Finally, the psychological perception of conventional form-factor plots tends to be dominated by their trivial Bessel-function aspects, which makes it difficult to detect the consequences of different choices for models of nuclear structure. We have, accordingly, chosen to display the form factors in a representation which removes much of these trivial q dependences.

In the limit of small values of the momentum transfer q, the spherical Bessel function in Eq.(6) can be expanded to exhibit explicitly the relation between the PWBA form factor and the gamma-transition matrix element M_p:

$$M_p = \lim_{q \to E_f - E_i} (2L+1)!!\ F_p(q) / q^L\ N_{F,P} \qquad (42)$$

This provides a well-known method for graphical comparisons of such matrix elements and form factors at small q values. We have chosen to remove, in addition, much of the trivial q dependence at larger q values by also dividing the complete inelastic form factors by the exponential dependence contained in harmonic-oscillator wave functions, namely, $\exp(-b^2q^2/4)$.

The effects on the E4 and E2 form factors of dividing the F(q) by these two functions of b and q are as follows. Since only the $\emptyset$d shell orbits contribute to the E4 model-space transition density, and in the oscillator model

$$R(\emptyset d,r) \alpha\ r^2 \exp(-r^2/2b^2) \tag{43}$$

$$A_4(r) \alpha\ r^2 \exp(-r^2/b^2) \tag{44}$$

we have in PWBA

$$F_{4,p}(q)/D_{HO,4}(b,q) = M_{4,p}\ , \tag{45}$$

where

$$D_{HO,L}\ (b,q) = N_{F,p}\ q^L \exp(-b^2q^2/4)(2L+1)!! \tag{46}$$

Hence, $F_{4,p}(q)$ divided by the quantity $D_{HO,4}$ is the matrix element $M_{4,p}$, which is independent of q. For the E2 form factor both 0d and 1s orbits contribute and division of $F_{2,p}(q)$ by D_{HO} gives

$$F_{L,p}(q)/D_{HO,L}(b,q) = M_{L,p}\{1 + (q^2b^2/4)[1 - 4R^2_{dtr,L}/(4L+6)]\} \tag{47}$$

(for sd shell, L=2)

$R_{dtr,L}$ is the dimensionless transition radius

$$R_{dtr,L} = R_{tr,L}/b \tag{48}$$

where $R_{tr,L}$ is the transition radius (a generalization of the root-mean-square radius), defined by

$$R^2_{tr,L} = \int r^{L+2}\rho(r)r^2dr / \int r^L\rho(r)r^2dr \tag{49}$$

For the PWBA reaction model and any transition density based on harmonic-oscillator wave functions, Eq. (47) gives the first two terms in a general expansion in q^{2L}. (It is implicitly understood that for the moment the values of b used for the HO potential and in the D function are the same.) The fact that the term proportional to q does not contribute for L = 4 means that $R^2_{dtr,4} = (11/2)$ in the sd shell. The plot of Eq. (47) against q^2 is a straight line. Since in practice only absolute values are measured, we plot all values as positive, which converts the E2 straight line into two straight lines which have their vertex at zero.

We wish to obtain the benefits of this sort of representation of form factors in all cases, not just for special HO results. To achieve this we will display all L = 2 sd-shell form factors after dividing the $F_{L,p}(q)$ values by the universal q- and L-dependent factors

$$D_L(q) = D_{HO,L}(b_0,q)\ \exp(b_0^2 q^2/4A)\ \exp(-0.43\ q^2/4) \qquad (50)$$

where b_0 is obtained from a global formula for the oscillator length which gives a smooth two-parameter fit to rms charge radii over the entire periodic table:

$$\hbar\omega_0 = 41.46/b_0^2 = 45\ A^{-1/3} - 25\ A^{-2/3} \qquad (51)$$

The second exponential in Eq. (50) accounts for the center-of-mass correction and the third exponential accounts for the nucleon finite-size correction in the one-Gaussian approximation. The alternate representations $F(q)^2$ and $M(q)$ for E2 and E4 form factors are shown in Fig. (2).

In discussing the many comparisons of theory to experiment in which we have plotted all form factors transformed according to

$$M(q) = \frac{|F(q)|}{D(q)} \qquad (52)$$

we will still use the term "form factor". Both theoretical and experimental form factors will have been divided by exactly the same factor and thus no additional assumptions will be involved in the comparison between experiment and theory. The ratios M(q) plotted

against q^2 for L=2 and L=4 sd-shell form factors will tend to be straight lines for the reasons discussed above. (The L=0 elastic form factors would be a quadratic function in the variable q^2 if plotted in this way). Small deviations from this nominal linearity will result from the differences between the actual center-of-mass and finite-size corrections and those used in Eq. (50). Larger deviations will result if the sd-shell radial wave functions are different from the $\hbar\omega_0$ oscillator wave functions used in the D(q) functions and/or if the core-polarization transition density has a shape which is different from the model-space transition density.

We note here a few of the simple features associated with the form factors in the point-nucleon, harmonic-oscillator-model approximation. In this limit the momentum transfer q and the oscillator length b always appear in the combination q^2b^2. Hence the shape of a form factor F(q) calculated with any value of b can be made equivalent to that calculated with another b value merely by rescaling q. This has the particular consequence that the magnitudes of the maxima of the form factors are independent of b.

This independence of the E2 form factor maximum value from the value of b in the HO-PWBA limit is equivalent in the practical case to an approximate independence of this maximum value from the effective nuclear radius. The B(E2) value, on the other hand, depends upon b or the equivalent parametrization of the rms radius to the fourth power. Accurate independent measurements of both

the B(E2) value for a transition and the E2 form factor thus hold the promise of allowing the effects of radial extent and coherent enhancement via configuration mixing of the one-body transition strengths to be disentangled.

For the highest electric multipolarity within a major shell (E4 in the case of the sd shell) the value of q at the maximum of the form factor F(q) is

$$q^2_{max} = (2L)/b^2 \qquad \text{(for sd shell, L=4)} \qquad (53)$$

and the value of the form factor at this value of q is

$$F(q_{max}) = N_{F,p} \left[M_p/b^L \right] (2L)^{L/2} \exp(-L/2) \,/(2L+1)!! \qquad \text{(for sd shell, L=4)} \qquad (54)$$

This value is actually independent of b since M_p is proportional to b^L. For the next highest multipolarity within a major shell (E2 for the sd shell) there are in general two maxima, at values of q which can be obtained from a quadratic equation involving both b and the transition radius. The value of q at the minimum between these two maxima can easily be obtained from Eq. (47):

$$q^2_{min} = -(4/b^2)[1 - 4\, R^2_{dtr,L}/(4L+6)]^{-1} \qquad \text{(for sd shell, L=2)} \qquad (55)$$

III. Comparisons of calculated form factors with experimental results

III.1. Introduction

The context of the present study does not include issues such as the validity of the impulse approximation, the contribution of non-nucleonic components in the nuclear wave functions and large-momentum-transfer phenomena in general. Within the present context, form-factor results depend on two dominant general assumptions, one explicit in conventional analyses, one implicit. The explicit assumption is the choice of model space. For the nuclei considered here we assume that the Øs and Øp shells are completely filled and that the shells above the sd shell are completely vacant. The implicit assumption is that the simple single-particle-potential model suffices to generate the radial components of the single-nucleon wave functions. To this is usually appended the vital subsidiary assumption that all of the single-nucleon wave functions for a given A-value are generated from a single parametrization of the chosen shape of this potential. (We refer to this as the "orbit-independent" hypothesis.) The final link in this chain of implicit assumptions is that the correct potential parametrization to use for the valence orbits when describing inelastic form factors is that which yields, under the foregoing assumptions, the best description of the elastic scattering. We will consider this last assumption in some detail.

At a more detailed level, different calculations of the form factor for a given transition are distinguished by the choice of the shell-model Hamiltonian, i.e., the resulting values of the matrix elements of the one-body transition density (OBDM), by the functional form ("shape") of the single-nucleon potential, by the parameter values of this form and, for an inelastic transition, by the shape and normalization of the core-polarization transition density. As was discussed in Sections II.2, II.3 and II.4, our considerations in this work are restricted to the shell-model wave functions of the USD Hamiltonian (in one sense we are attempting to test the predictions of this calculation), to single-nucleon wave functions principally of the harmonic-oscillator and Woods-Saxon forms, and to core-polarization transition densities whose shapes are given either by the shape of the valence transition density itself or by the Tassie model. The size normalizations of the HO single-nucleon wave functions are chosen here either to yield a fit to the ground-state rms radius of the nucleus in question or to the shape of an inelastic E2 form factor itself. The normalizations of the core-polarization transition densities are chosen either to have average values dictated by systematics or values chosen to fit the measured B(E2) values for given transitions.

For the typical sd-shell nucleus, the choice of the active model orbits and the Hamiltonian-dependent predictions of occupation probabilities and OBDM matrix elements are the best validated of the various ingredients which must be combined in the calculation of a form factor. That is, the uncertainties associated with these aspects

are most objectively established, being calibrated and tested with a diversity of experimental data which are independent not only of electron scattering but of EØ, E2 and E4 data in general. In the context of the shell-model calculation, an elastic form factor depends only upon the occupation probabilities of the orbits. Inelastic form factors involve specific configuration-mixing effects in a more complex fashion, in that both their shapes and their magnitude scales depend upon the OBDM values.

The magnitude scale of a theoretical inelastic form factor depends upon both the individual magnitudes and the overall coherence properties of the OBDM matrix elements for the transition and upon the normalization of the core-polarization transition density term. In particular, these quantities determine the magnitudes of the first E2 and E4 maxima in the typical "strong" form factors. (As noted in Section II.6, these values in the HO-PWBA model limit are independent of the rms radius of the transition density.) In the simplest idealization of the nuclear shell model, these maximum values would be correctly predicted by the OBDM matrix elements in conjunction with a state- and mass-independent normalization of the core-polarization term. However, more sophisticated treatments of the core-polarization corrections suggest strong state dependencies in their normalizations. It is therefore not clear how much significance should be attached to small deviations from experimental magnitudes of theoretical form factors which do assume a constant normalization for the core-polarization term.

The qualitative shape of E2 form factors in the sd-shell space can be related simply to the magnitude and phase of the net "d" to "d" one-body transition amplitude relative to that of the net "d" to "s" term, as is described in Ref 16. This formulation encompasses both the collective-type E2 form factors observed in both experiment and theory for all of the 0+ to first 2+ transitions and most of the 0+ to second 2+ transitions and the qualitatively different shapes such as that measured and calculated for the 0+ to second 2+ transition of ^{20}Ne. The most easily specified feature of the "collective-type" E2 shape is the location of the intercept with zero following the first maximum, which gives a measure of the relative expansion or contraction of the diffraction pattern with respect to the momentum-transfer scale. The qualitative shape of the E4 form factors is invariant for sd-shell calculations since only the "d" to "d" one-body transition term contributes.

We will see that the changes in the shell-model wave functions which would be required to correct the largest discrepancies which are found between the shapes of the diffraction-pattern structure of experimental and "standard" theoretical inelastic form factors are qualitatively inconsistent with the consensus of the spectroscopic data for the region. On the other hand, as we will discuss in the following paragraphs, these discrepancies are easily corrected by small changes in the radial dimensions of the single-nucleon wave functions. Thus, the assumptions which determine the radial sizes of

the single-nucleon wave functions are most important in determining the degree of correspondence between the diffractive-structure aspects of experimental and theoretical form factors. At the same time, they are the least susceptable to independent experimental verification.

Even for doubly-closed-shell systems, the description of light nuclei in terms of an orbit-independent single-nucleon potential of the HO, WS or equivalently concise form is almost certainly overly simplistic. The assumption cannot be verified experimentally in any case, only not disproved. For open-shell nuclei any such model suffers in addition from the intrinsic defect that the intra-shell correlation energies (the shell-model two-body energy contributions) are not taken into account, so that the separation energies of the valence orbits are incorrect relative to experiment. In ^{28}Si, for example, the radial parameters of the wells set according to the interpolation described in Section II.3 yield proton single-particle energies of -8.25, -5.38 and -3.87 MeV for the $0d_{5/2}$, $1s_{1/2}$ and $0d_{3/2}$ orbits, respectively. We will refer to such single-nucleon wave functions as originating from an orbit-independent Woods-Saxon (WSOI) potential model.

The measured separation energies of the protons in the ^{28}Si ground state are considerably larger than the WSOI predictions, being about -13 MeV for all orbits. This to be understood, as mentioned, in terms of the many-body correlations which fall outside the compass of the single-nucleon potential model. The overall underestimation of the

binding energies can be remedied by altering the well parameters. The discrepancy between calculated and measured spectra of separation energies, however, is congenital to the single-particle model except in the case of closed-shell nuclei. This is of fundamental importance because the decrease in magnitude of a radial wave function at large radius is governed by the separation energy The "centroid" energies obtained with the WSOI potential therefore give incorrect radial tails. There is no definitive method for obtaining a single-nucleon potential for open-shell nuclei which produces more realistic radial behavior. We have explored the consequences of one of the more commonly used prescriptions, namely that of adjusting the WS well depth independently for each orbit so as to reproduce the required separation energies. We will refer to this as the Woods-Saxon orbit-dependent (WSOD) potential model.

In the remainder of this section we first (Section III.2) survey the degree of accuracy with which the elastic scattering data pertinent to the inelastic transitions of interest can be reproduced with the sd-shell occupation probabilities of Table (3) and the various models for the single-nucleon wave functions which we consider. We next (Section III.3) inspect the general effects of the size and shape of the single-nucleon wave functions and the choice of model for the core-polarization transition density upon the features of calculated form factors. For these studies we principally use the concisely specified HO potential to generate the single-nucleon wave

functions and compare selected exmples to calculations with Woods-Saxon single-nucleon wave functions. We then compare (Sect. III.4) various parametrizations of the HO-based form factors to experimental examples for which measurements have been made over a significant range of momentum transfers. The aim in this section is to obtain the best agreement possible between theory and experiment within the confines of the assumption of HO radial dependence. From these fits we are also able to test the consistency of the measured values of B(E2) with the measured form factors, again within the context of the HO model. Finally, in Section III.5, we review the existing data on E2 and E4 transitions in the sd-shell in comparison to "standard" theoretical form factors. The calculations in these last comparisons employ the empirically suggested mass- and state-independent E2 and E4 effective-charge normalizations previously noted and size normalizations based either on the measured ground-state radii (HO results) or on the parameters obtained an interpolation between the ^{16}O and ^{40}Ca values (WS results).

All of our comparisons between calculated E2 form factors and (e,e') data are made with reference to the measured values (Ref 44, Ref 45), where they exist, of B(E2) for the transitions. We list in Table (5) the experimentally determined values of $[(2J_i + 1)B(E2)]^{1/2}$ for the transitions of concern here, together with the theoretical values obtained with the "standard" HO and WS calculations mentioned above. These experimental values are displayed in all of the figures which show (e,e') E2 data.

III.2. Dependence of calculated elastic scattering form factors upon the model chosen for the single-nucleon potential

Measured elastic form factors for ^{16}O, ^{40}Ca and the A = 20-36 nuclei of present concern are shown in Fig. (3) in comparison with DWBA calculations which incorporate single-nucleon wave functions of harmonic oscillator (HO) potentials with $b=b_{rms}$ (solid lines), of orbit-independent Woods-Saxon (WSOI) potentials with interpolated parameters (dashed lines), and of Skyrme-Hartree-Fock (SHF) potentials (dot-dashed lines). The predictions for ^{16}O and ^{40}Ca assume perfect shell closures while those for the A = 20-36 nuclei assume a perfect ^{16}O shell closure and the sd-shell occupation probabilities of Table 3. Out to q = 3 fm^{-1}, the diffraction features are correctly reproduced and the magnitudes are reproduced to within about a factor of two at the worst by any of the three sets of results. At momentum transfer values greater than 2 fm^{-1}, the HO and WSOI results resemble each other more closely than either of them resemble the SHF results and the SHF results are, overall, in poorer agreement with the data.

At momentum transfer values less than about 2 fm^{-1}, all three formulations of the potential yield similar results. In most examples, the HO results fall below the WSOI results and the data in

the region of the second diffraction maximum, 1.2-2.0 fm^{-1}. However, there are many details in which the HO results are superior to the particular alternatives considered here. On the basis of the comparisons shown in Figure (3) we will omit further discussion of results based on the SHF potential. Study of their impact upon inelastic form factors reveal nothing significantly different from the corresponding HO and WS results.

We do not think these comparisons justify a conclusion that the WS formulation is qualitatively superior to the HO formulation in describing the radial properties of ground states as manifested in elastic scattering data, contrary to the conclusions of Ref 17 and Ref 16. Insofar as these data are concerned, the virtue of the WS formulation relative to that of the HO lies in the greater freedom the WS parametrization allows in adjusting the relative values of the various orbits of the core and valence spaces. We conclude that the dominance of the radial dependences of the single-nucleon wave functions in the elastic form factor results makes it impossible to draw quantitively firm conclusions about the orbit occupation probabilities. Moreover, the importance of the core orbits and their behaviors at small radii also makes it impossible to establish the radial dependences of the valence orbits unambiguously on the basis of these data.

III.3. Dependence of calculated form factors upon the size parameter of harmonic-oscillator single-nucleon wave functions, upon the relative differences between harmonic-oscillator and Woods-Saxon forms and upon the model assumed for the core-polarization transition density

We illustrate the dependence of form factors upon the radial "sizes" assumed for single-nucleon wave functions and upon the model assumed for the core-polarization transition densities with calculations for the elastic scattering and the inelastic scattering to the first 2+ and 4+ states, in ^{28}Si. Our aim is to determine the range of variation in shape which can result from combining a single shell-model prediction with a variety of prescriptions for these auxiliary aspects of form-factor calculations. We utilize the single-nucleon wave functions of the harmonic-oscillator (HO) potential model and, as a starting point, assume a value of the size parameter b that reproduces the measured rms radius of the nucleus we consider. The solid curve in Figure (4) shows the elastic form factor for ^{28}Si calculated (DWBA) with the shell-model occupation probabilities of the present shell-model calculation and the HO length parameter $b = b_{rms} = 1.813$ fm. Its agreement with experiment can be noted in Fig. (3).

The dotted and dashed lines indicate the corresponding form factors calculated with b values increased and decreased by 5%, respectively, from the b_{rms} value. The differences in the form factors which result from this magnitude of parameter variation are clearly evident relative to the data. The effects of configuration mixing between the the d and s orbitals of the model space upon the elastic form factor also can be inferred from inspection of Figure (4) by comparing the solid line with the dot-dashed line, which shows the form factor calculated with $b = b_{rms}$ but with the jj-coupling limit of 12 $d_{5/2}$ nucleons in the ^{28}Si ground state rather than the predicted mixture given in Table (3). These predicted occupation probabilities yield a ratio of 0.13 for the s-state to d-state occupancy within the sd-shell. We can thus infer from Fig. (4) that in the context of a given set of assumptions, the elastic scattering data can yield information on the relative s-state occupancies at the level of a few percent.

The solid curve in Figure (5) shows the form factor of the 0+ to 2+ inelastic transition calculated with the $b = b_{rms}$ HO model and the Tassie model for the core-polarization transition density, normalized to $e_p + e_n = 1.7e$. The dashed line in this figure shows the form factor of the same transition, calculated with the same HO model but with the valence instead of the Tassie model for the core-polarization term, again normalized to $e_p + e_n = 1.7e$. The dot-dashed and dotted lines, respectively, show the corresponding form factors calculated with the length parameter of the HO potential

reduced from b_{rms} by 5%. Note that in our formulation the Tassie-model term is the same for both the b = b_{rms} and the b = b_{rms} - 5% calculations, since it is based on the parametrized empirical ground-state charge distribution (Ref 40) and our assumption of $e_p + e_n = 1.7e$. The valence-model term, on the other hand, changes its profile as b is varied exactly as does its parent, model-space transition density. The four curves in Figure (6) show the form factors of the 0+ to 4+ transition calculated with the same two HO potentials and same two models for the core-polarization transition density which were used in the 0+ to 2+ calculations shown in Figure (5), with the exception that the normalization for the effective charge is taken to be $e_p + e_n = 2.0e$, rather than 1.7e.

From consideration of these results, the characteristic dependence of the form factors upon the "nuclear size", and the sensitivity of this dependence can be inferred. In the valence model, the effects of a 5% smaller radius upon the E2 results is seen to be a 10% decrease in the square root of B(E2), a 10% increase in the q-value at which the pure HO result intersects zero, and larger values of the form factor at higher q-values. For E4 transitions, the same decrease of radius reduces the square root of the B(E4) by 20% and increases the form factor at larger q-values. The use of the Tassie model in place of the valence model for the core-polarization transition density results in slightly smaller magnitudes between the photon point (at which the Tassie and valence results are normalized to each other) and the zero-intercept point and more significant decreases

in magnitudes at q^2-values beyond about 4 fm^{-2}.

We now turn to the question of what differences typically result from substituting single-nucleon wave functions from a Woods-Saxon potential for those of the HO potential. The solid lines in Figures (7) and (8) show the form factors for the same 0+ to 2+ and 0+ to 4+ transitions of ^{28}Si just studied in the context of the HO assumption as now calculated with single-nucleon wave functions of the WSOI potential in combination with the Tassie model. The dashed lines show the form factors calculated with the same single-nucleon wave functions in combination with the valence model. The 0+ to 2+ results use an effective-charge normalization of $e_p + e_n = 1.7e$ and the 0+ to 4+ results use a normalization of $e_p + e_n = 2.0e$. The results of similar calculations with the WSOD potential are shown in Figures (7) and (8) by the dot-dashed lines for the Tassie model and the dotted lines for the valence model.

The increase in the single-nucleon binding energies obtained in going from the WSOI to the WSOD potential has the expected effect of decreasing the size of the valence radii (the total rms radius changes from 3.238 fm to 3.147 fm) and hence increasing the position of the first minimum in the 0+ to 2+ form factor. This change goes in the direction of improving the agreement with experiment in the particular case of ^{28}Si, but in general this formulation is in no better systematic agreement with experiment than is the HO or the WSOI

formulation. Since the WSOD single-nucleon wave functions, with their large values for single-nucleon binding energies, are quite similar in shape to the HO wave functions, we choose to display in the remainder of our discussion the WSOI results, so as to achieve the maximum diversity of form-factor behavior.

The characteristic differences between results based alternatively on the HO and WS models can be inferred from comparisons between Figures (5) and (7) for E2 and between Figures (6) and (8) for E4. Aside from differences which are simply attributable to the small differences in the various total rms radii, the HO and WS results are very similar.

III.4 Comparison of thoroughly-measured form factors with calculations which incorporate harmonic-oscillator single-nucleon wave functions

The examples shown in Figures (4), (5) and (6) provide the backdrop for our comparisons of experimental form factors with HO-based calculations. The data we consider, principally from Ref. 40, Ref. 46, Ref. 47 and Ref. 48, are for the ground state to first excited state, 0+ to 2+ transitions in ^{24}Mg, ^{28}Si and ^{32}S, the 0+ to 4+ (6.00 Mev) transition in ^{24}Mg and the 0+ to 4+ (4.62 MeV) transition in ^{28}Si. Extensive measurements by several groups, extending over a relatively wide range

of momentum transfer values, make these examples particularly suitable as a proving ground for our calculations. The data for an individual transition from different sources are not always mutually consistent, however. We have emphasized the Stanford data (Ref 40) in most instances when choosing which calculations "best fit" experiment.

We compare the data for each of the 0+ to 2+ transitions to form factors calculated with two different HO potentials. The value of b for one potential is taken to be b_{rms} and the the value for the other to be $b_{t\lambda r}$. The value of $b_{t\lambda r}$ in each case is obtained by visually optimizing the fit of the calculated form factor to the data out to values of q^2 of about 4 fm^{-2}. With each of these models for the single-nucleon wave functions we combine, in turn, the Tassie and valence models for the core-polarization term. The effective-charge normalization for each form factor in each instance is set here to reproduce the measured value of B(E2).

The solid line in Figure (9) shows the E2 form factor calculated for ^{24}Mg with $b=b_{rms}$ and the Tassie model. The dashed line shows the form factor calculated with the same HO potential and the valence model. The dot-dashed and dotted lines in Figure (9) show, respectively, form factors calculated with the Tassie and valence models in combination with HO potentials whose b values are adjusted to achieve in each example, as mentioned above, an optimum match between the calculation and the data. The value of $b_{t\lambda r}$ depends slightly upon the model chosen for the core-polarization term, as

could be inferred from the differences between the two lines showing the results obtained with $b = b_{rms}$. The same four types of E2 form-factor calculations are shown in Fig. (1Ø) for ^{28}Si and in Fig. (11) for ^{32}S. The values of b_{rms}, b_{f2+} and $e_p + e_n$ used in all of these cases are listed in Table (6).

The calculations with b_{rms} for ^{24}Mg and ^{28}Si are seen to fail below the data throughout the region of the first diffraction maximum and, as follows, to have their intersects with zero at too-small values of q. The corresponding ^{32}S calculations do not exhibit this behavior. The ^{24}Mg and ^{28}Si results are symptomatic of theoretical radii which are too large. The values obtained for b_{f2+} give quantitative estimates of just how much.

We see from these comparisons that the form factors obtained with the $b = b_{f2+}$ HO potentials are in very good agreement with both the measured B(E2) values and with the Stanford data out to at least $q^2 = 4$ fm^{-2}. We recall that the E2 form factor calculated in DWBA differed from the corresponding PWBA calculation principally in that the PWBA results were too low in the region of the minimum. Hence the tendency for the calculations to fall below the data points in this region of momentum transfer can be attributed merely to a PWBA effect.

We conclude that the combination of the shell-model matrix elements with the HO model for the single-nucleon wave functions and either model for the core-polarization term can produce good fits simultaneously to both the B(E2) data and the form factor data at low and intermediate values of momentum transfer if the b value and the effective charge normalization are adjusted slightly from their standard values to achieve such fits. Significant discrepancies between theory and experiment only begin to appear at momentum transfers greater than 6 fm^{-2}. In the present study we attach only marginal significance to phenomena at momentum transfers beyond this point, since experimental results may be affected significantly by effects not in our model's compass and within the model's context the calculations depend very sensitively upon cancellations between external and internal features of the transition densities.

Since for Ø+ to 4+ transitions we do not have B(E4) values at the photon point, we do not attempt to adjust the effective-charge normalizations used in the E4 form factor calculations. In Figures (12) (^{24}Mg) and (13) (^{28}Si) we show, in comparison with the data, form factors calculated with the effective-charge normalization $e_p + e_n = 2.0e$ and the HO parameters $b = b_{rms}$ and $b = b_{f2+}$. The solid lines show the form factors obtained with the Tassie model and the HO potential with $b = b_{rms}$. The dashed lines show the results obtained with the valence model and the same single-nucleon wave functions. The dot-dashed lines show the form factors calculated from the combination of the Tassie model and a $b =$

$b_{f2+,T}$ HO model. The dotted lines show the results obtained from the assumptions of the $b = b_{f2+,V}$ single-nucleon wave functions and the valence model for the core-polarization transition density.

The smaller b values which were suggested by the E2 form factors in these nuclei are seen here to move the E4 form factors in the wrong directions relative to the data. In the context of the valence model, b values larger, not smaller, than b_{rms} would yield improved fits to the E4 data. In the context of the Tassie model, however, the values $b = b_{rms}$ provide good fits.

Results have been previously obtained, equivalent to those shown in Fig (12), which yielded discrepancies between the experimental data for the second 4+ transition in ^{24}Mg and a form factor calculated with antecedant shell-model functions, the valence model and an orbit-independent, ground-state-consistent single-nucleon potential (Ref 18). On the basis of these discrepancies it was argued in Ref 18 that the correct structure of the second 4+ state in ^{24}Mg is such that the matrix element of the "extra-model-space" one-body-transition $\emptyset d_{5/2}$ to $\emptyset g_{9/2}$ is larger than the net intra-model-space $\emptyset d$ to $\emptyset d$ matrix element.

This conclusion, based on choosing the two amplitudes of the $\emptyset d_{5/2}-\emptyset d_{5/2}$ and the $\emptyset d_{5/2}-\emptyset g_{9/2}$ one-body transition densities so as to fit the observed form factor, is of course, totally

dependent on the accuracy of the experimental data and of the assumptions which must be made about which one-body terms to include in such a fit and about their radial dependencies.

Certainly, it is true both that these data, as noted, suggest that some effective "enlargement" of the "standard" radius for the $\emptyset d$ to $\emptyset d$ transition density is needed to construct the correct radial profile of the total transition density for this case. It is also true that an ad hoc addition of a $\emptyset d$ to $\emptyset g$ contribution of the optimum magnitude to the transition density will accomplish this enlargement. The core-polarization term of the conventional shell-model approach must involve $\emptyset g$ excitations and they are probably more heavily weighted in the E4 corrections than in the E2 corrections. However, there are significant differences between a single-nucleon transition density such as the $\emptyset d$ to $\emptyset g$ term and the coherent sum of many $2\hbar\omega$ terms which is presumed to create the core-polarization term and these should be testable in some instances, such as by measurement of $g_{9/2}$ stripping strength.

At any rate, the sort of "configuration analysis" used in Ref 18 should not be confused with shell-model analyses such as we are studying here. The former cannot be objectively related to the general run of spectroscopic phenomena because of its intrinsic ad hoc nature, specific to just these (e,e') data. In the shell-model approach, the various non-electron-scattering data bearing on this state, such as excitation energy and nucleon-transfer and beta-decay

strengths, are accounted for consistently with the shape and strength of the E4 form factor. Moreover, the description of this 4+ transition is seen to be consistent with that of the 4+ transitions in ^{20}Ne and ^{28}Si and the description of the 4+ states with that of many, many other states. The extensiveness of this net of relationships is the essential virtue of the shell-model approach to understanding experimental phenomena. In this context we consider the results shown in Fig. (12) as constituting a signal confirmation of the efficacy of the present shell-model calculations rather than as evidence that the single-nucleon structure of this state is significantly different from that predicted by the present calculation.

We conclude from the results shown in Figures (12) and (13) that E4 form factors which incorporate the Tassie model for the core polarization are in better agreement with the data than are those which incorporate the valence model. This preference of the data for the Tassie-based results is consistent with a similar, though less definitive, preference for the Tassie-based E2 results in the region of momentum transfers beyond the vertex points. On these grounds we conclude that the Tassie-model shape is superior to the valence shape as a mechanism for introducing core-polarization effects into the shell-model form-factor calculations.

III.5. Comparison of experimental form factors with calculations which incorporate Tassie core-polarization models, constant effective-charge normalizations, and single-nucleon wave functions of the HO ($b = b_{rms}$) and WSOI models

In this section we present "standard" calculations for the form factors of the inelastic excitations to the first and second 2+ and 4+ states in the doubly-even nuclei A = 20-36 and compare them with the available data. We aim here at studying the global trends of theory and experiment and their relationships rather than at achieving, by manipulation of parameters, the closest possible agreement between theory and experiment in individual cases. For each transition we show two form-factor predictions, one based upon single-nucleon wave functions of the WSOI potential model and the other upon the $b = b_{rms}$ parametrization of the HO potential model. We have concluded from the results presented in Section III.4 and III.5 that the Tassie model for the core-polarization transition density is preferable to the valence model and here we show here only the Tassie-model results. Since we want to emphasize systematic trends we use the previously noted constant values for the effective-charge normalizations of $e_p + e_n = 1.7e$ for E2 and $e_p + e_n = 2.0e$ for E4.

In Figure (14) we show measured (Ref 49, Ref 50, Ref 51) and calculated form factors for the first two 2+ states of ^{20}Ne. The calculated and observed shapes for the first 2+ are in good agreement with each other and are similar to the shapes of the first 2+ states of ^{24}Mg, ^{28}Si and ^{32}S which we have

already studied in Section III.4. Also, the measured B(E2) value, the magnitudes of the measured form factor and the two predictions are mutually in good accord. The observed shape of the form factor for the 2+ state at 7.43 MeV is completely different from that familiar from the lowest 2+ transitions. The calculated shapes for this transition agree well with the measured shape although the very small calculated magnitudes are too large by a factor of two. The B(E2) value is unmeasured. The anomalous character of this transition and its qualitative reproduction by an antecedant version (Ref 21) of the present shell-model calculation has been noted previously (Ref 19). The form factors calculated for the first two model 4+ states of ^{20}Ne are shown in Fig. (15). Data are available only for the first 4+ state (Ref 49). The shape of the HO calculation is in better agreement with the observed shape than is that of the WSOI calculation. The HO results are about 10% too low, and the WSOI results about 20% too low, in the region of the greatest statistical accuracy of the data.

In Figure (16) we show measured (Ref 50, Ref 52) and calculated form factors of the first two 2+ states of ^{22}Ne. For the first 2+ transition, the magnitudes of the calculated and measured form factors and the measured B(E2) value are mutually in good agreement. The slight decrease in strength observed for this ^{22}Ne transition relative to that of the transition to the first 2+ in ^{20}Ne is accurately reproduced theoretically. The shape of the measured form factor tends to be "flatter" than theory, but

inconclusively so. The form factor measured for the second 2+ state in ^{22}Ne has magnitudes about a factor of five smaller than those of the first 2+ and, similar to the stronger transition, its shape has a less-steep negative slope than that of the calculated shapes. The theoretical magnitudes of the second 2+ form factor are larger than the experimental values by about a factor of two. The B(E2) value is unmeasured. The form factors calculated for the first two 4+ states of ^{22}Ne are shown in Fig. (17). A few data are available for the first of these states (Ref 52) and the calculated form factors are in satisfactory agreement with them.

In Figure (18) we show measured (Ref 53, Ref. 46 Ref 40, Ref 48) and calculated form factors of the first two 2+ states of ^{24}Mg. These particular model shapes are in only qualitative agreement with the data between q^2 = 1 and 3 fm^{-2}. As was observed in the discussion of this transition in Section III.4, almost all of this discrepancy in detail can be removed by using smaller radii for the model-space single-nucleon wave functions. The shape and magnitudes measured for the form factor of the second 2+ state, together with the B(E2) value, are well reproduced by the two calculations. Relative to the ^{20}Ne 0+ to 2+ transitions, these data show a small increase in the strength of the first state and a "normal", that is to say "similar to the first 2+ state" form factor for the second 2+ state, unlike the "anomalous" second 2+ state in ^{20}Ne. All of these observed trends are reproduced by the calculations.

The measured (Refs. 48, 53, 46, and 40) and calculated form factors of the first and second 4+ states of and calculated form factors of the first and second 4+ states of ^{24}Mg are shown in Figure (19). The weak transition to the first 4+ state has an observed (Ref 48) shape which is completely different from the calculated shapes. The anomalous nature of these data relative to any conventional sd^{n} calculation has been noted previously (Ref 48). The calculated magnitudes for this transition are considerably lower than the measured values at lower q values. It would seem worthwhile to make a quantitative estimate of the possible multistep contributions to the observed cross sections for this state, since both the 0+ to 2+ and 2+ to 4+ E2 transitions are strongly enhanced. The observed shape and magnitudes of the form factor of the strong transition to the second 4+ state are, as was discussed in Section III.4, in good agreement with the calculations if at the lowest momentum transfers only the data of Ref 46 are considered.

In Figure (20) we show measured (Ref 54) and calculated form factors for the first two 2+ states in ^{26}Mg. For both transitions, the calculated form factors agree with the average magnitudes of the data and with the measured B(E2) values. However, the observed shapes have a less-steep negative slope than is shown by the calculations, a result similar to that found in ^{22}Ne. Relative to the analogous transitions in ^{24}Mg, both the measured and calculated strengths of each of these transitions in ^{26}Mg are

reduced. The calculated form factors for the first two 4+ states of ^{26}Mg, predicted to be of comparable strength, are shown in Figure (21) in comparison to the few available data (Ref 55).

In Figures (22) and (23) we show the measured (Ref 44, Ref 47, and Ref 40) and calculated form factors of the first two 2+ and 4+ states of ^{28}Si. Electron scattering data are available only for the lowest state of each spin and comparisons between theory and experiment for these cases have been discussed extensively in earlier sections. The shape of the calculated form factor for the second 2+ state, as was the case for ^{20}Ne and will be the case for ^{36}Ar, is different from the "collective" shape usually observed in both calculation and experiment. The calculated and measured B(E2) values for this state are both quite small, but differ by a factor of two. As in the case of ^{26}Mg, the first two 4+ transitions are predicted to have comparable strengths.

In Figure (24) we show measured (Ref 55) and calculated form factors for the lowest two 2+ states in ^{30}Si. The measured B(E2) value, the average magnitudes of the form factor data and the calculations are mutually in good agreement for the first 2+ state. The qualitative features of the relationship between theory and experiment for the second 2+ state are the same as for the first 2+. In detail, the calculated magnitudes are 15% too

large relative to the measured $(B(E2))^{\frac{1}{2}}$ value and the low-q form-factor data. The relationship of the theoretical ^{30}Si results to the corresponding ^{28}Si results is reminiscent of the relationship between the analogous pairs of E2 transitions in ^{22}Ne and ^{20}Ne. The data, insofar as they exist, are in agreement with these trends. Predictions for the lowest two 4+ states in ^{30}Si are shown in Fig. (25). Again, they are predicted to have comparable strengths.

In Figures (26) and (27), respectively, we show measured and calculated form factors for the lowest two 2+ and 4+ states in ^{32}S. Electron scattering data are available (Ref. 40) only for the lowest 2+ state, and their relationship to the theoretical results has been discussed in Section III.4. The predicted B(E2) values are fairly close to the measured values for both states.

In Figures (28) and (29), respectively, we show calculated form factors for the lowest two 2+ and 4+ states in ^{34}S. Form-factor data for these transitions are unavailable. The measured B(E2) values are in good agreement with the photon-point values of the predictions. The shell-model wave functions predict that the 0+ and 2+ transitions in ^{34}S stand in the same relationship to those of ^{32}S as do those of ^{26}Mg to those of ^{24}Mg.

In Figures (30) and (31), respectively, we show calculated form factors for the lowest two 2+ and 4+ states in ^{36}Ar. Form-factor data are unavailable for these transitions. The calculated B(E2) values are in good agreement with the measured value for the first 2+ transition but are significantly smaller than experiment for the second 2+. The predicted form factors for the second 2+ transition have a shape similar to that noted for the second 2+ states in ^{20}Ne and ^{28}Si.

IV. Recapitulation

We have reviewed here only a few of the many varieties of form factors which can be constructed upon the foundation of our sd-shell, USD Hamiltonian shell-model one-body-transition-density matrix elements. In order to calculate form factors from these OBDM matrix elements it is necessary to specify the radial forms of the single-nucleon wave functions and of the radial form and normalization of the appropriate core-polarization component of the total transition density. We have studied examples in which the shell-model predictions are combined with single-nucleon wave functions from one or the other of two standard potential models and with one or the other of two simple models for the core-polarization transition density. These particular models are chosen because of their ease of use and their conventionality and because, in conjunction, they span a broad range of conceivable nuclear behavior.

The HO potential was chosen because it has great analytical advantages and eliminates many ambiguities in the state and orbit dependence of the radial wave functions. Its infinite depth produces the radial behavior we expect in the limit for tightly-bound systems. The finite-depth WSOI potential was studied as an alternative to the HO potential since its loose binding of the higher shell-model orbits produces radial behavior at the other extreme, in a certain sense, from the HO results. The valence model for the core-polarization

transition density strongly emphasizes the role of the shell-model eigenfunctions in the total form factor. The alternative Tassie model, with its state-independent, collective-type shape, moderates the influence of particular single-particle-like features in the model-space transition densities.

We did not exhaustively study the various possible formulations of elastic form factor calculations. The shell-model components of such calculations are minimal (for our sd-shell calculations they amount to the net ratio of the $1s_{1/2}$ to $0d_{5/2}$ plus $0d_{5/2}$ occupancies). And, upon reflection, it will be realized that there exist an endless succession of equivalently plausible, equivalently unrealistic single-nucleon-potentials to investigate. Finally, the link between the properties of individual single-nucleon wave functions in the ground-state, even if ascertainable, and those appropriate for inelastic transitions is itself uncertain. We chose the harmonic-oscillator and Woods-Saxon formulations for investigation because they are typically the ones considered in this sort of study. From our comparisons of experiment with the elastic form factors calculated from these models we see little basis for describing one formulation as clearly superior to the other. Neither formulation would seem to merit the adjective "realistic", and both would seem to offer qualitatively adequate prescriptions for generating the single-nucleon wave functions.

Better agreement between experimental and theoretical elastic

form factors obviously can be obtained by relaxing the orbit-independence constraint and adjusting the radial scale of each single-nucleon wave function independently. This procedure would preclude testing the predictions of the shell-model calculations, of course. In any case, however, such tests are extremely dependent upon the assumptions which define the radial features of these wave functions and, with respect to such tests, we conclude only that the orbit occupancies predicted by our shell-model wave functions are merely not in significant disagreement with the elastic-scattering data.

From comparisons of the various versions of calculated inelastic scattering form factors with experimental data it appeared that the Tassie-model shape was superior to the valence-model shape as a vehicle for introducing core-polarization effects. This conclusion rested primarily upon the analysis of the E4 form factors and, to a lesser degree, upon the analysis of E2 form factors in the region of the second diffractive maximum.

We generated systematic sets of "standard" inelastic form-factor predictions which incorporated the Tassie model core-polarization term by constraining the single-nucleon wave functions for a given A-value to originate from a common potential (either HO or WSOI) which was parametrized to yield a reproduction within our model of the radial properties of that ground state and by constraining the effective-charge normalizations of the E2 and E4 core-polarizatior

transition densities to have the shell-wide, constant values of $e_p + e_n = 1.7e$ and $2.0e$, respectively. These predictions agree quite well with the available data on the whole. The shapes of all observed E4 form factors except that of the very weak first 4+ state in ^{24}Mg are well fitted and the magnitudes are in agreement to within about 10%. The qualitative shapes of observed E2 form factors are consistently well reproduced by the calculations, which usually, but not always, are similar to the typical pure-collective-model form factor. Agreement in magnitudes is within 10%, or 2 e fm^2, for the strong transitions to the first 2+ states and within 50%, or the same 2 e fm^2, for the weak to very weak transitions to the second 2+ states.

The discrepancies observed between the magnitude scales of these standard calculations and the experimental form factors are very similar to deviations between measured B(E2) values and the predictions of these same and similar calculations. It is difficult to assess the importance of discrepancies of the observed magnitudes since they exist in the context of the assumption of a mass- and state-independent effective-charge normalization. Theoretical expectations of the state dependence of the effective charge normalizations suggest greater variations than in fact are needed to bring the shell-model predictions into perfect accord with experiment. Resolution of this issue extends beyond electron scattering per se, in any case, and we content ourselves with merely defining the quantitative features of the problem as it is manifested in the

present examples.

The unique nuclear structure information embodied in electron scattering data is manifested in the variation of inelastic scattering cross sections with momentum transfer, that is to say, in the "shapes" of the form factors. We have displayed this information in terms of functions M(q) from which much of the universal size and reaction-mechanism effects upon the q dependence of the cross sections are removed. The usual $F(q)^2$ representation of form factors emphasizes their diffractive structure aspects. We think that the M(q) representation emphasizes their basic nuclear-structure contents and significantly enhances our ability to understand and assess the important constituent elements of these phenomena.

All transitions observed to have form factors which at least qualitatively resemble the usual collective-model shape are also predicted to have this shape by the present calculations. The dominant discrepancies in detail between the "shapes" of these calculations and the "shapes" observed experimentally can be expressed in terms of different scales in momentum transfer of the calculated and measured form factors, or, equivalently, of different radial scales of the transition densities.

These discrepancies are most evident in the form factors of the first 2+ states of ^{24}Mg and ^{28}Si, for which the "standard" theoretical radial scales appear to be too large by about 5%, rather

independent of any "reasonable" variations within the assumed model context. Problems of this sort are not so evident in the somewhat less thoroughly measured form factors of ^{20}Ne and ^{32}S. The form factor data on other transitions do not span a large enough range of momentum transfer values to illuminate this issue further. By contrast, in the context of the valence model for the core-polarization term (but not, we emphasise, in the context of the alternative Tassie model) the theoretical radial scales for the strong E4 transitions appear to be about 5% too small in these same nuclei.

Remedies to the existing deficiencies in the "standard" shell-model descriptions of the radial scales of transition densities can be sought alternatively in the contexts of different, perhaps state-dependent, radial scales of the underlying single-nucleon wave functions of the model space, of different, perhaps state-dependent, radial dependences for the core-polarization transition densities and of different values of OBDM matrix elements. In this last context we can distinguish between values of the model-space OBDM which are different from those obtained in the shell-model calculation and non-zero values of extra-model-space OBDM. It is important to realize that to a significant degree all three of these remedial procedures overlap in the basic physical effects they attempt to introduce.

In studying the discrepancies between theoretical and experimental form factors we have concentrated on the simplest remedy,

namely the alteration of the radial scales of the single-nucleon wave functions of the model space from the values suggested by fitting the elastic scattering data within the confines of an orbit-independent single-nucleon potential model. For unambigousness, we kept a single scale for all the OBDM terms of a given transition even though there is some rationale for small variations here also. We have argued that the over-simplifications inherent in describing open-shell nuclei with any conventional single-particle model create some justification for relaxing the constraint of a single well parametrization for all occupied and partially-occupied orbits.

For E2 form factors we showed that contractions of the radial scales of the single-nucleon wave functions of the order of 5% or less, coupled with variations of similar magnitudes in the effective-charge normalizations, sufficed to yield agreement of calculation with experiment to beyond 2 fm^{-1} in momentum transfer to within experimental uncertainties, and qualitative agreement on out to 2.5 fm^{-1}. These fits were perfectly consistent with the independent measurements of B(E2).

For E4 form factors, we saw that expansions of the radial scale were required to remove the discrepancies between experiment and the calculations which incorporated "standard" radii and the valence model for the core polarization term. These discrepancies between experiment and theory did not appear when the the Tassie model instead of the

valence model was use for the core polarizational term. Because of angular momentum selection rules, different single-particle orbits enter into the E2 and E4 core-polarization corrections. The differences between the E4 and E2 results thus are suggestive of differences in detail between the E2 and E4 core polarizations which were not part of our simple formulation. It is possible that microscopic calculations of these terms will eventually account for the "inconsistencies" revealed in the analysis.

V. Conclusions

We have reviewed the observed shapes and magnitudes of the inelastic electron scattering form factors of the 0+ to 2+ and 4+ transitions in A = 20-36 nuclei, emphasizing their dependences upon mass and state. We compared these phenomena with calculations based on shell-model wave functions augmented with assumptions of simple state- and mass-independent core-polarization terms and single-nucleon wave functions consistent with observed ground-state radii. The general trends of the data out to about 2.5 fm^{-1} momentum transfer were reproduced by these calculations. At momentum transfers higher than 2.5 fm^{-1}, theory and the few extant data diverged markedly. The residual discrepancies between experiment and theory are best discussed in terms of additive corrections to the magnitudes and multiplicative scalings of the momentum transfer axis. Such

discrepancies were of the order of about 1-2 e fm^2 for magnitudes, which corresponds to 5-10% in $B(EL)^{1/2}$ for strong transitions and 20-50% for weak transitions. Expansions or contractions of the radial scales of the single-nucleon wave functions and core-polarization terms sufficient to remove the q-scale discrepancies in form-factor shapes were of the order of 5% in the worst cases.

More and better experimental measurements are necessary if the present type of analysis is to yield unambiguous answers as to the independent roles of the shell-model wave functions, single-nucleon wave functions and core-polarization components of the theoretical form factors beyond the levels of precision established here. As is evident from Figs. 14-30, measurements exist for only about half of the 2+ and 4+ transitions covered in our analysis. In principle, a particular strength of the shell-model theory is its ability to account self-consistently for the observed variations in phenomena associated with changes in nucleon number and excitation energy. Without measurements of a significantly larger number of transitions, this vital critique can not be throughly applied to the present sd-shell predictions. Existing measurements on many transitions amount to a few data points around 1 fm^{-1}. For the present sort of analyis we need precise data from q = 0.4 to 2.5 fm^{-1} in order to be able to focus on the shape of the core-polarization component and the radial scale. Finally, in the few transitions for which extensive measurements are available, sets of data from different sources seem

to have an unacceptably large scatter relative to each other. Hence, some precise experimental normalization points would be valuable even for ^{24}Mg and ^{28}Si.

Our conclusions from this study are that longitudinal E2 and E4 electron scattering data out to 2.5 fm^{-1} are consistent with the predictions of a complete and unified shell-model treatment of the nuclear structure of the nuclei between ^{16}O and ^{40}Ca. This consistency is, of course, relative to the present state of experimental knowledge and theoretical understanding. Agreement between theory and experiment for these phenomena confirms that the theoretical wave functions incorporate the correct patterns of quadrupole and hexadecupole collectivities down to rather precise detail. Comparisons of theoretical with experimental shapes confirm that the radial dependences of the single-nucleon-wave-function building blocks of the multiparticle shell-model wave functions are basically correct, although their precise sizes seem, in the context of the present analysis at least, to be state dependent at the level of 5%. Measurements with modern facilities on these nuclei could quickly improve the present state of experimental knowledge on this topic and allow a significantly more rigourous and detailed critique of the present theoretical approach.

ACKNOWLEDGEMENTS: This work has been supported in part by Grant PHY-80-17605 from the U.S. National Science Foundation. We wish to express our apreciation to Jim Banks for his help in preparing the manuscript and to Orilla McHarris and Mamar Blosser for their efficient and accurate realizations of the figures.

FIGURE CAPTIONS:

Fig (1): PWBA form factors of the 0+ to first 2+ and 0+ to first 4+ transitions of ^{28}Si calculated with the pure Tassie model (dashed line) and with the Bohr-Mottelson model (solid line). The data are taken from Ref 55(diamonds), Ref 47(triangles) and Ref 40((circles) 250 MeV and (squares) 500 MeV). The M(q) vs q representation is explained in Section II.6.

Fig (2): DWBA form factors for the elastic scattering and the 0+ to first 2+ and 0+ to first 4+ inelastic scattering transitions of ^{28}Si (solid lines), in comparison with PWBA form factors for the same transitions (dashed lines). The calculations incorporate the shell-model one-body-transition-density matrix elements, harmonic-oscillator single-nucleon wave functions with $b = b_{rms}$ and the valence model for the core-polarization transition density. The E2 and E4 form factors are displayed both in the conventional $F(q)^{\lambda}$ vs. q representation and the M(q) vs. q representation explained in Section II.6.

Fig (3): Elastic form factors measured for ^{16}O (Ref 56, (circles)-374.5 MeV and (squares)-750 MeV), ^{20}Ne (Ref 57, (triangles) and Ref 58, (circles), ^{24}Mg (Ref 46 (triangles),(Ref 40(circles)-250 Mev and (squares)-500 MeV)), ^{28}Si (Ref 47 (triangles), Ref 40 (circles)-250 MeV and (squares)-500 MeV), ^{32}S (Ref 47 (triangles), Ref 40 (circles)-250MeV and (squares)-500 MeV), ^{36}Ar (Ref 59) and ^{40}Ca (Ref 60 and Ref 61) compared with DWBA calculations which incorporate single-lnucleon wave functions of the harmonic oscillator (HO) potentials with values of b = b (solid lines), the Woods-Saxon orbit-independent (WSOI) potential (dashed lines) and the Skyrme-III-interaction Hartree-Fock potential(dot-dashed lines).

Fig (4): DWBA elastic form factors for ^{28}Si calculated with HO single-nucleon wave functions of three different values of b: $b = b_{rms} = 1.827$ fm (solid line), $b = b_{rms} + 5\%$ (dotted line) and $b = b_{rms} - 5\%$ (dashed line), respectively. The effects of removing the configuration mixing between the d and s orbitals predicted by the shell-model wave functions are shown by the dot-dashed line, as calculated with $b = b_{rms}$.

Fig (5): Form factors of the 0+ to first 2+ transition of ^{28}Si calculated with the HO model, $b = b_{rms}$, combined with the Tassie model normalized to $e_p + e_n = 1.7e$ (solid line) and with the HO model, $b = b_{rms}$,combined with the valence model normalized to $e_p + e_n = 1.7e$ (dashed line). The corresponding form factors calculated with $b = b_{rms} - 5\%$ are shown, respectively, by the dot-dashed and the dotted lines.

Fig (6): Form factors of the 0+ to first 4+ transition of ^{28}Si calculated with the HO model, b = b_{rms}, combined with the Tassie model normalized to $e_p + e_n = 2.0e$ (solid line) and with the HO model, b = b_{rms}, combined with the valence model normalized to $e_p + e_n = 2.0e$ (dashed line). The corresponding form factors calculated with b = b_{rms} - 5% are shown, respectively, by the dot-dashed and the dotted lines.

Fig (7): Form factors for the 0+ to first 2+ transition of ^{28}Si The calculations incorporate single-nucleon wave functions obtained from the Woods-Saxon orbit-independent (WSOI) and and Woods-Saxon orbit-dependent (WSOD) potentials in combination with the Tassie and valence models for the core-polarization models. The combination of WSOI and Tassie models is shown by the solid line, that of WSOI and valence by the dashed line, that of WSOD and Tassie by the dot-dashed line and that of WSOD and valence by the dotted line. The effective-charge normalization of 1.7e in used in each case.

Fig (8): Form factors for the 0+ to first 4+ transition of ^{28}Si. The calculations use the same models for single-nucleon wave functions and polarizations-charge transition density, and are presented with the same conventions, as those described in the caption to Fig. (7) The effective-charge normalization is taken to be 2.0e in each case.

Fig (9): Form factors of the 0+ to first 2+ transition of ^{24}Mg. The calculations incorporate single-nucleon wave functions of a HO potential with b = b_{rms} combined with the Tassie and valence models (solid and dashed lines, respectively) and of HO potentials with individually-fitted b values again combined with the Tassie and valence models (dot-dashed and dotted lines, respectively). In each case the core-polarization normalization is chosen to reproduce the measured B(E2) value. The data are taken from Ref 53 (diamonds), Ref 46 (triangles) and Ref. 40 ((circles)-250 MeV and (squares)-500 MeV).

Fig (10): Form factors of the 0+ to first 2+ transition of ^{28}Si. The calculations are analogous to, and are identified with the same conventions as, those presented in Fig. (9). The data are identified as described in the caption to Fig. (1).

Fig (11): Form factors of the 0+ to first 2+ transition of ^{32}S. The calculations are analogous to, and are identified with the same conventions as, those presented in Fig. (9). The data are taken from Ref 47 (triangles) and Ref 40 ((circles)-250 MeV and (squares)-500 MeV).

Fig (12): Form factors for the 0+ to first 4+ transition of ^{24}Mg. The calculations use the same HO single-nucleon wave functions and core-polarization transition density models as those described in the caption to Fig. (9) except that here the effective-charge

normalizations are set to 2.0e in each case. The results and the data are presented in the same conventions as those used in Fig. (9)

Fig (13): Form factors for the 0+ to first 4+ transition of ^{28}Si. The calculations are analogous to those described in the caption to Fig. (12) and are presented, along with the data Ref 47 (triangles), according to the same conventions.

Fig (14): Form factors for inelastic electron scattering to the first two 2+ states of ^{20}Ne. The calculations shown incorporate the Tassie model normalized to 1.7e combined with single-nucleon wave functions of the HO potential, b = b_{rms} (solid lines) and of the WSOI potential (dashed lines). The data are taken from Ref 49 (triangles), Ref 50 (circles), and Ref 51 (diamonds).

Fig (15): Form factors for inelastic electron scattering to the first two sd-shell 4+ states of ^{20}Ne. The calculations shown incorporate the Tassie model normalized to 2.0e combined with single-nucleon wave functions of the HO potential, b = b_{rms} (solid lines) and of the WSOI potential (dashed lines). The data are taken from Ref 49 (triangles).

Fig (16): Form factors for inelastic electron scattering to the first two 2+ states of ^{22}Ne., The calculations and the conventions of their presentation are as described in the caption to Fig. (14). The data are taken from Ref 50 (circles) and Ref 52 (triangles)

Fig (17): Form factors for inelastic electron scattering to the first two 4+ states of ^{22}Ne. The calculations and the conventions of their presentation are as described in the caption to Fig. (15). The data are taken from Ref 52 (triangles).

Fig (18): Form factors for inelastic electron scattering to the first two 2+ states of ^{24}Mg. The calculations and the conventions of their presentation are as described in the caption to Fig. (14). The data are taken from Ref 53 (diamonds), Ref 46 (triangles), Ref 40 ((circles)-250MeV, (squares)-500 MeV) and Ref 48 (x's).

Fig (19): Form factors for inelastic electron scattering to the first two 4+ states of ^{24}Mg. The calculations and the conventions of their presentation are as described in the caption to Fig. (15). The data are taken from Ref 48 (x's), Ref 53 (diamonds), Ref 46 (triangles) and Ref 40 ((circles)-250 MeV, (squares)-500 MeV).

Fig (20): Form factors for inelastic electron scattering to the first two 2+ states of ^{26}Mg. The calculations and the conventions of their presentation are as described in the caption to

Fig. (14). The data are taken from Ref 54 (triangles).

Fig (21): Form factors for inelastic electron scattering to the first two 4+ states of ^{26}Mg. The calculations and the conventions of their presentation are as described in the caption to Fig. (15). The data are taken from Ref 54 (triangles).

Fig (22): Form factors for inelastic electron scattering to the first two 2+ states of ^{28}Si. The calculations and the conventions of their presentation are as described in the caption to Fig. (14). The data are taken from Ref 55 (diamonds), Ref 47 (triangles) and Ref 40 ((circles)-250 MeV, (squares)-500 MeV).

Fig (23): Form factors for inelastic electron scattering to the first two 4+ states of ^{28}Si. The calculations and the conventions of their presentation are as described in the caption to Fig. (15). The data are taken from Ref 47 (triangles).

Fig (24): Form factors for inelastic electron scattering to the first two 2+ states of ^{30}Si. The calculations and the conventions of their presentation are as described in the caption to Fig. (14). The data are taken from Ref 55 (triangles).

Fig (25): Form factors for inelastic electron scattering to the first two 4+ states of ^{30}Si. The calculations and the conventions of their presentation are as described in the caption to Fig. (15).

Fig (26): Form factors for inelastic electron scattering to the first two 2+ states of ^{32}S. The calculations and the conventions of their presentation are as described in the caption to Fig. (14). The data ate taken from Ref 47 (triangles) and Ref 40 ((circles)-250 MeV, (squares)-500 MeV).

Fig (27): Form factors for inelastic electron scattering to the first two 4+ states of ^{32}S. The calculations and the conventions of their presentation are as described in the caption to Fig. (15).

Fig (28): Form factors for inelastic electron scattering to the first two 2+ states of ^{34}S. The calculations and the conventions of their presentation are as described in the caption to Fig. (14).

Fig (29): Form factors for inelastic electron scattering to the first two 4+ states of ^{34}S. The calculations and the conventions of their presentation are as described in the caption to Fig. (15).

Fig (30): Form factors for inelastic electron scattering to

the first two 2+ states of ^{36}Ar. The calculations and the conventions of their presentation are as described in the caption to Fig. (14).

Fig (31): Form factors for inelastic electron scattering to the first two 4+ states of ^{36}Ar. The calculations and the conventions of their presentation are as described in the caption to Fig. (15).

Table (1). Calculated one-body transition density matrix elements for 0+ to 2+ transitions in the A = 20-36, doubly-even sd-shell nuclei and the calculated and observed excitation energies of the #th 2+ states.

					OBDM(i,f,L=2, ΔT,j,j')							
A	#th	Energy		2j-2j' =	5-5	5-1	5-3	1-5	1-3	3-5	3-1	3-3
		theor.	expt.	ΔT								
20	1	1.776	1.634	0	0.4010	0.4399	0.0882	0.3757	0.1533	-0.1032	-0.2177	0.0947
20	2	7.316	7.421	0	-0.4356	0.2509	-0.0333	0.1901	0.0667	0.0360	-0.0887	-0.0587
22	1	1.368	1.275	0	0.9582	0.5943	0.3261	0.6954	0.2073	-0.3341	-0.2472	0.0886
				2	0.1315	-0.0657	0.1809	0.0368	0.0287	-0.1634	0.0045	-0.0037
22	2	4.455	4.457	0	0.1153	0.1140	-0.1031	0.0830	-0.0117	-0.0503	-0.1433	0.1142
				2	-0.4801	0.0307	0.0239	0.0094	-0.0705	-0.1243	0.0793	0.0510
24	1	1.509	1.369	0	-0.6176	-0.3232	-0.3197	-0.4255	-0.1523	0.3155	0.1473	-0.0553
24	2	4.122	4.238	0	0.1700	0.0552	0.0990	0.0609	-0.0799	-0.2739	-0.0065	0.1850
26	1	1.928	1.809	0	-0.7413	-0.4637	-0.4391	-0.7477	-0.2172	0.5178	0.2299	-0.1636
				2	0.4883	-0.0480	0.0199	-0.0355	0.0228	0.0232	-0.0010	-0.0274
26	2	3.153	2.938	0	-0.1991	-0.2543	-0.0880	-0.5505	0.0610	0.1738	0.0205	-0.1249
				2	-0.2432	-0.1008	-0.0650	-0.3644	-0.0514	0.0367	0.0632	-0.0200
28	1	1.987	1.779	0	-0.2986	-0.4066	-0.3038	-0.5949	-0.0862	0.3835	0.1532	-0.1714
28	2	7.522	7.381	0	0.3404	-0.1165	0.0775	-0.2493	-0.1849	-0.1730	0.2166	0.0205
30	1	2.310	2.235	0	0.2367	0.4115	0.3605	0.7305	0.3998	-0.4440	-0.6724	0.1917
				2	-0.0199	-0.1612	0.0083	-0.2669	0.2989	0.0123	-0.4604	0.1132
30	2	3.550	3.499	0	0.1088	0.2213	0.1632	0.5182	0.0141	-0.4030	0.1363	-0.1452
				2	-0.1251	-0.0227	0.0127	-0.2547	-0.0482	-0.1715	0.2381	-0.2722
32	1	2.148	2.230	0	-0.0701	-0.1542	-0.1105	-0.2155	-0.3730	0.1178	0.6000	-0.2492
32	2	4.353	4.282	0	0.0906	0.1547	0.1557	0.2620	0.0456	-0.4069	-0.0516	-0.1443

34	1	2.200	2.127	0	-0.1329	-0.1900	-0.1937	-0.2534	-0.4536	0.2794	0.8482	-0.6594
				2	0.0245	0.0214	0.0767	0.0148	0.0257	-0.0428	-0.1444	-0.5439
34	2	3.138	3.303	0	0.0521	0.0066	0.0232	0.0130	-0.0850	-0.2090	0.5077	0.0995
				2	0.0285	-0.0232	-0.0336	0.0177	0.1760	0.1050	-0.5870	0.4644
36	1	1.927	1.970	0	0.0833	0.1049	0.0811	0.1401	0.2572	-0.1457	-0.3726	0.6582
36	2	4.410	4.440	0	0.0093	-0.0812	0.0325	-0.1018	-0.2360	-0.0373	0.3541	0.5551

Table (2). Calculated one-body transition density matrix elements for 0+ to 4+ transitions in the A = 20-36, doubly-even sd-shell nuclei and the calculated and observed excitation energies of the #th 4+ states.

					OBDM(i,f,L=4, ΔT,j,j')		
A	#	Energy		2j-2j' =	5-5	5-3	3-5
		theor.	expt.	Δ T			
20	1	4.123	4.248	0	-0.4106	-0.2507	0.2931
20	2	9.974	9.990	0	0.0601	-0.1177	0.0955
22	1	3.378	3.357	0	-0.0318	-0.2130	0.3408
				2	0.6331	0.0360	-0.0692
22	2	5.480	5.523	0	0.8062	-0.0284	-0.1532
				2	0.3944	-0.0780	-0.0169
24	1	4.379	4.123	0	0.2961	-0.0362	0.1017
24	2	5.935	6.010	0	0.2394	0.2739	-0.4697
26	1	4.532	4.318	0	-0.7226	-0.0334	0.2019
				2	0.5500	-0.1073	0.1477
26	2	4.932	4.900	0	0.0903	0.3365	-0.7909
				2	0.0074	0.0330	-0.1782
28	1	4.659	4.617	0	-0.0032	-0.2413	0.4981
28	2	7.037	6.889	0	0.2137	0.1289	-0.4659
30	1	5.506	5.280	0	-0.2593	-0.3573	0.9770
				2	0.0724	-0.1073	0.2254
30	2	5.913	5.950	0	-0.0035	-0.1778	0.6246
				2	-0.0420	0.1097	-0.4522
32	1	4.698	4.459	0	-0.0819	-0.2690	0.5603
32	2	6.265	6.411	0	-0.0844	-0.1294	0.4013

34	1	4.896	4.688	0	-0.1061	-0.3570	0.8430
				2	0.0210	0.0045	-0.1385
34	2	6.819	6.729	0	0.0688	0.1339	-0.4848
				2	0.0330	0.0377	-0.0702
36	1	4.564	4.414	0	0.0734	0.2342	-0.4024
36	2	6.357	6.356	0	-0.0317	-0.0732	0.1743

Table (3). Calculated occupation numbers for the sd-shell orbits in the ground states of the A = 20-36 even-mass nuclei.

A	p/n	2j= 5	1	3
20	p=n=	1.21	0.51	0.28
24	p=n=	2.99	0.45	0.56
28	p=n=	4.62	0.70	0.68
32	p=n=	5.42	1.42	1.16
36	p=n=	5.54	1.78	2.68
22	p=	1.40	0.42	0.18
22	n=	3.18	0.39	0.43
26	p=	3.20	0.35	0.45
26	n=	4.82	0.56	0.62
30	p=	4.74	0.68	0.58
30	n=	5.15	1.41	1.44
34	p=	5.61	1.66	0.73
34	n=	5.76	1.76	2.48

Table (4). Experimentally determined rms charge radii of stable sd-shell-nuclei and the corresponding values calculated in the harmonic-oscillator model with length parameters b_{rms} and in Woods-Saxon and Skyrme models.

NUCLEUS	rms(fm) exp	b(fm)	Exp.Ref	rms(fm) HO	rms(fm) WSOI	rms(fm) SKIII
16 O	2.720(40)	1.769	a	2.728	2.715	2.714
20 Ne	3.020(20)	1.869	c	3.027	2.999	2.974
22 Ne	2.949(21)	1.822	d	2.935	2.927	2.939
24 Mg	3.035(18)	1.813	e	3.043	3.127	3.075
26 Mg	3.017(32)	1.802	c	3.022	3.079	3.060
28 Si	3.125(3)	1.827	b	3.134	3.238	3.171
30 Si	3.137(15)	1.835	g	3.147	3.205	3.186
32 S	3.263(2)	1.881	b	3.272	3.334	3.285
34 S	3.264	1.881		3.312	3.275	3.303
36 AR	3.399(5)	1.938	g	3.405	3.411	3.397
40 Ca	3.474(3)	1.963	e	3.480	3.477	3.484

a) Ref 62

b) Ref 63

c) Ref 64

d) Ref 65

e) Ref 40

f) Ref 66

e) Ref 67

h) Ref 68

Table (5). Measured and calculated values of E2 transition strengths from the 0+ ground states to the first and second 2+ states in the stable, even-mass nuclei from A = 20 through A = 36.

Nucleus		$[(2J_i + 1)B(E2)]^{1/2}$, 0+ to 2+		
		expt.	theory	
			HO, b_{rms}	WSOI
20 Ne	1	17.09(1.07)	16.44	17.87
	2		0.38	0.28
22 Ne	1	15.12(0.29)	15.18	15.97
	2		4.45	4.59
24 Mg	1	20.71(0.21)	18.64	20.42
	2	4.73(0.23)	5.57	6.01
26 Mg	1	17.58(0.31)	17.33	18.45
	2	3.02(0.18)	2.99	3.28
28 Si	1	18.09(0.26)	18.51	19.99
	2	2.95(0.37)	1.09	1.43
30 Si	1	14.25(0.40)	14.06	14.72
	2	6.47(0.29)	7.89	8.19
32 S	1	17.33(0.32)	14.94	15.43
	2	6.65(0.48)	7.49	7.66
34 S	1	13.96(0.29)	12.79	12.90
	2	4.88(0.18)	4.76	4.79
36 Ar	1	17.28(0.75)	15.65	15.30
	2	3.74(0.35)	1.09	1.07

Table 6. Values obtained for the oscillator length paramenter b = b_{f2+} and effective-charge normalization $e_p + e_n$ in fitting HO form factors to experimental data for the first 2+ states of ^{24}Mg, ^{28}Si and ^{32}S.

Nucleus	b_{rms}	b_{f2+}		e_p+e_n	
		Tassie	valence	Tassie	valence
24 Mg	1.813	1.70	1.76	2.15	2.00
28 Si	1.827	1.75	1.80	1.81	1.70
32 S	1.881	1.88	1.90	1.97	1.93

References:

1. T. de Forrest and J. D. Walecka, Adv. Phys. 15, 1 (1966)
2. J. L. Friar and J. W. Negele, "Adv. in Nuclear Physics", edited by M.Baranger and E.Vogt (Plenum, New York, 1975), Vol. 8, p. 219
3. H. Uberall, "Electron Scattering from Complex Nuclei" (Academic Press, New York, 1971)
4. R. Hofstadter, Rev. Mod. Phys. 28, 214 (1964)
5. J. P. Cavedon et al. Phys. Rev. Lett. 49, 978 (1982)
6. T. W. Donnelly and J. D. Walecka, Nucl. Phys. A201, 81 (1973)
7. S. K. Platchkov et al., Phys. Rev. C25, 2318 (1982)
8. W. C. Barber, Ann. Rev. Nucl. Sci. 12, 1 (1962)
9. H. Theissen, Spinger Tracts in Modern Physics, vol. 65, (Springer-Verlag, Berlin, Heidelberg, New York; 1972)
10. J. Heisenberg, "Adv. in Nuclear Physics", edited by J. Negele and E.Vogt (Plenum, New York, 1982), Vol. 8, p. 61
11. L. J. Tassie, Austr. Jour. Phys. 9, 407 (1956)
12. R. H. Helm, Phys. Rev. 104, 1466 (1956)
13. E. C. Halbert, J. B.McGrory, B. H. Wildenthal and S. P Pandya, "Adv. in Nuclear Physics", edited by M. Baranger and E. Vogt, (Plenum, New York; 1971)
14. M. G. Mayer and J. H. D. Jensen, "Elementary Theory of Nuclear Shell Structure (Wiley, New York; 1955)
15. G. R. Hammerstein, D. Larson and B. H. Wildenthal, Phys. Lett. 39B, 176 (1972)
16. R. P. Singhal et al., Nucl. Phys. A323, 91 (1979)
17. R. P. Singhal et al., Phys. Lett. 68B, 133 (1977)
18. R. P. Singhal et al., Phys. Lett. 72B, 152 (1977)
19. R. P. Singhal et al., Phys. Lett. 76B, 170 (1978)

20. B. M. Preedom and B. H. Wildenthal, Phys. Rev. C6, 1633 (1972)

21. W. Chung, Ph. D. Thesis, Michigan State University (1976)

22. B. H. Wildenthal, Bull. Am. Phys. Soc. 27, 725 (1982)

23. R. S. Willey, Nucl. Phys. 40, 529 (1963)

24. T. de Forest, Jr. and J. D. Walecka, Adv. Phys. 15, 1 (1966)

25. T. W. Donnelly and J. D. Walecka, Ann. Rev. Nucl. Sci. 25, 329 (1975)

26. A.R. Edmonds, "Angular Momentum in Quantum Mechanics" (Princeton Univerity Press, 1960)

27. L. J. Tassie and F. C. Barker, Phys. Rev. 111, 940 (1958)

28. B. A. Brown, W. Chung and B. H. Wildenthal, Phys.Rev. C22, 774 (1980)

29. H. Chandra and G. Sauer, Phys. Rev. C13, 245 (1976)

30. W. Bertozzi, J. Friar, J. Heisenberg and J. W. Negele, Phys. Lett. 41B, 408 (1972)

31. B. A. Brown, W. Chung and B. H. Wildenthal, Phys. Rev. 21, 2600 (1980)

32. C. B. Dover and N. Van Giai, Nucl. Phys. A190, 373 (1972)

33. M. Beiner, H. Flocard, N. Van Giai and P. Quentin, Nucl. Phys. A238, 29 (1975)

34. B. A. Brown et al., Phys.Rev. C26, 2247 (1982)

35. D. Vautherin and D.M. Brink, Phys. Rev. C5, 626 (1972)

36. B. A. Brown, unpublished

37. B. H. Wildenthal, Proceedings of the Conference on Nuclear Structure and Particle Physics, Oxford, April 6-8, 1981, p. 85 (Institute of Physics)

38. B. A. Brown, A. Arima and J. B. McGrory, Nucl.Phys. A277, 77 (1977)

39. V.R. Brown and V.A. Madsen, Phys. Rev. C11, 1298 (1975)

40. C. G. Li, M. R. Yearian, and I. Sick, Phys. Rev. C9, 1861 (1974); I. Sick, private communication.

41. A. Bohr and B. R. Mottelson, Nuclear Structure Vol II, (New York, Benjamin 1975)

42. MIT Bates Laboratory and M. V. Hynes, private communication.

43. S. T. Tuan, L. E. Wright and D. S. Onley, Nucl. Inst. and Methods 60, 70 (1968)

44. P. M. Endt, At. and Nuclear Data Tables 23, 3 (1979)

45. K. Dybal et al., Nucl. Phys. A359, 431 (1981)

46. P. Junk, Ph.D. Thesis, Naturwise. Fak. der Johannes Gutenberg-Universitate zu Mainz (1970)

47. G. Mulhaupt, Ph.D. Thesis, Naturwise. Fak. Der Johannes Gutenberg-Universitate zu Mainz (1970).

48. H. Zarek et al., Phys. Lett. 80B, 26 (1978)

49. Y. Horikawa et al., Phys. Lett. 36B, 9 (1971)

50. R. P. Singhal et al., Can. J. Phys. 51, 2125 (1973)

51. S. Mitsunobu and Y. Torizuka , Phys. Rev. Lett. 28, 920 (1972)

52. X. K. Maruyama et al., Phys. Rev. C19, 1624 (1979)

53. A. Johnston and T. E. Drake, J. Phys. A7, 898 (1974)

54. E. W. Lees et al., J. Phys. A7, 936 (1974)

55. S. W. Brain et al., J. Phys. G3, 821 (1977)

56. I. Sick and J. S. McCarthy, Nucl. Phys. A150, 631 (1970)

57. Y. Horikawa , Prog. Theo. Phys. 47, 867 (1972)

58. E. A. Knight et al., J. Phys. G7, 1115 (1981)

59. J. M. Finn et al. Nucl. Phys. A274, 28 (1976)

60. B. B. P. Sinha et al., Phys. Rev. C7, 5 (1973)

61. I. Sick et al., Phys. Lett. 88B, 245 (1979)

62. M. Miska et al., Phys. Lett. 83B, 165 (1979)

63. L. A. Schaller et al., Nucl. Phys. A300, 225 (1978)

64. C. W. de Jager, H. de Vries, and C. de Vries, At. Data Nucl. Data Tables 14, 479 (1974).

65. R. P. Singhal, H. S. Caplan, J. R. Moreira, and T. E. Drake, Can. J. Phys. 51, 2125 (1975).

66. H. Euteneuer et al., Phys. Rev. C16, 1703 (1977)

67. R. Engfer et al., At. Data Nucl. Data Tables 14, 509 (1974)

68. W. J. Briscoe and H. Crannell, Proceedings of the International Conference on Nuclear Physics with Electromagnetic Interactions, Mainz, 1979 (Springer, Berlin, 1979), p. 2.6.

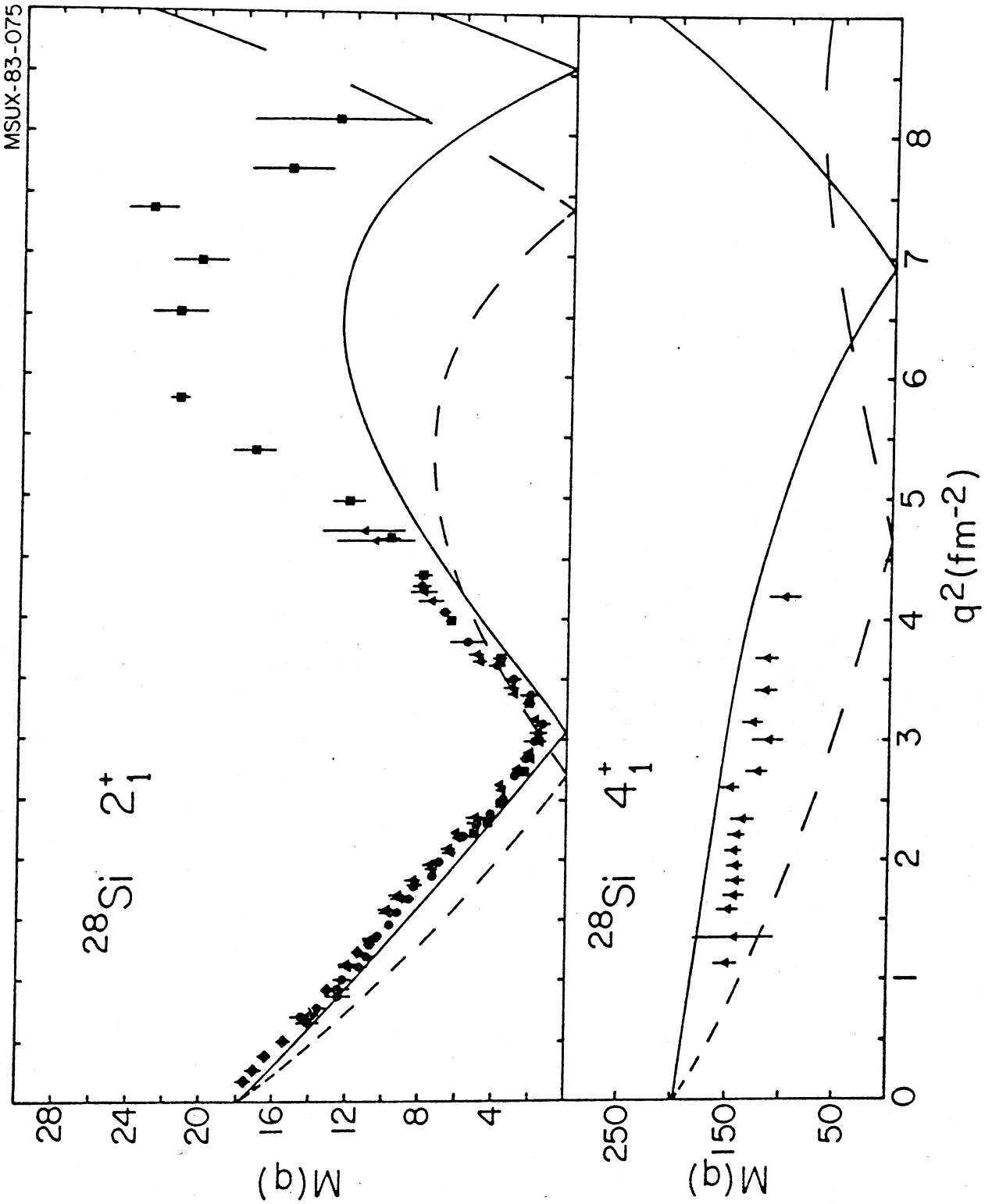

Fig. 1

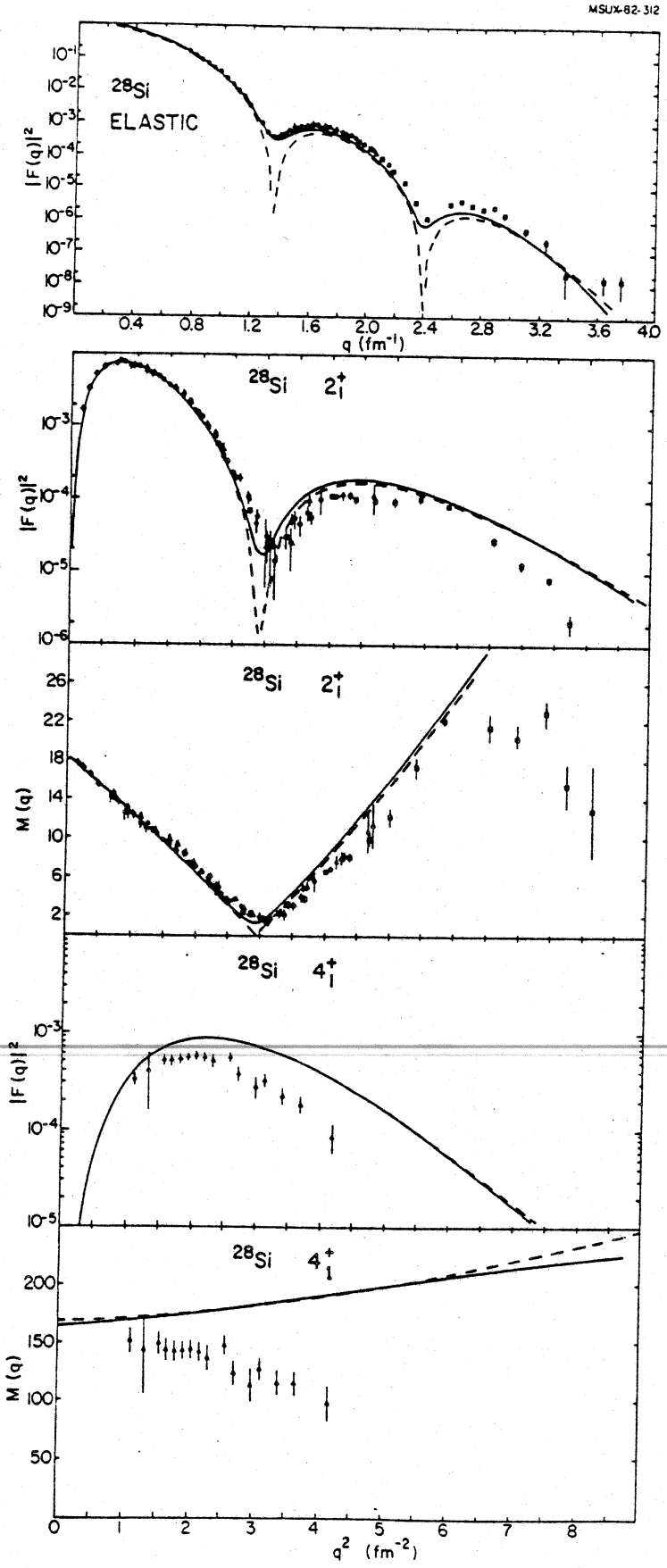
28Si
ELASTIC
|F(q)|²
q (fm⁻¹)
28Si 2₁⁺
|F(q)|²
28Si 2₁⁺
M(q)
28Si 4₁⁺
|F(q)|²
28Si 4₁⁺
M(q)
q² (fm⁻²)

Fig. 2

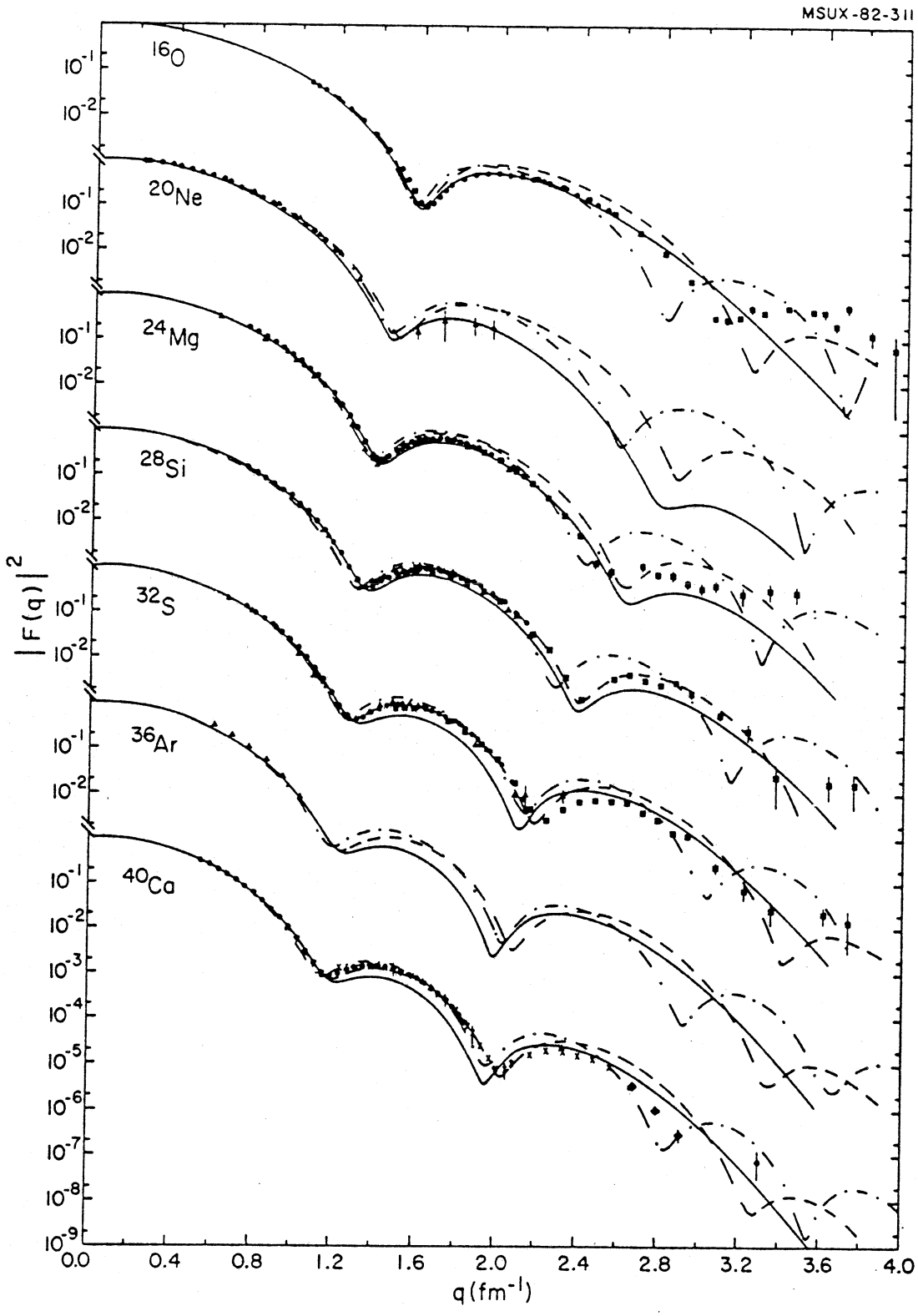
MSUX-82-311
^{16}O
^{20}Ne
^{24}Mg
^{28}Si
^{32}S
^{36}Ar
^{40}Ca
$|F(q)|^2$
$q(fm^{-1})$
0.0
0.4
0.8
1.2
1.6
2.0
2.4
2.8
3.2
3.6
4.0

Fig 3

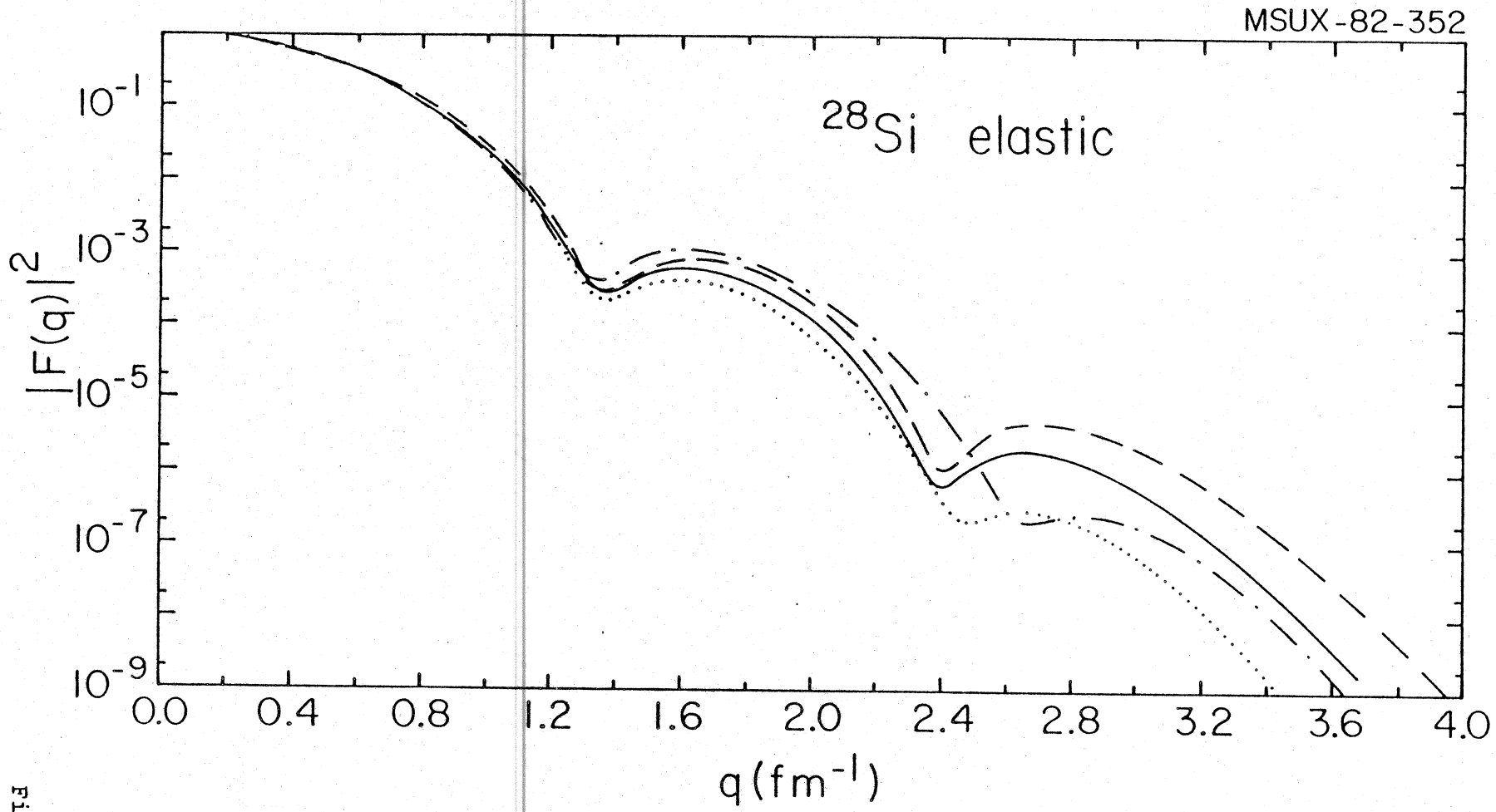
MSUX-82-352
^{28}Si elastic
$|F(q)|^2$
10^{-1}
10^{-3}
10^{-5}
10^{-7}
10^{-9}
0.0
0.4
0.8
1.2
1.6
2.0
2.4
2.8
3.2
3.6
4.0
q(fm^{-1})

Fig 4

MSUX-83-088

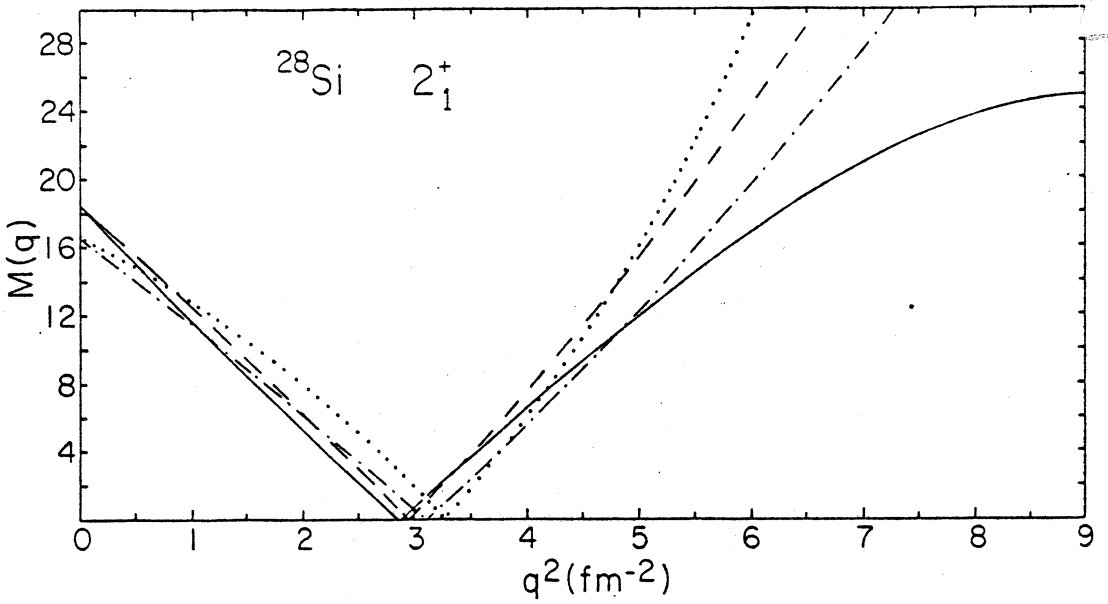

Fig. 5

MSUX-82-344

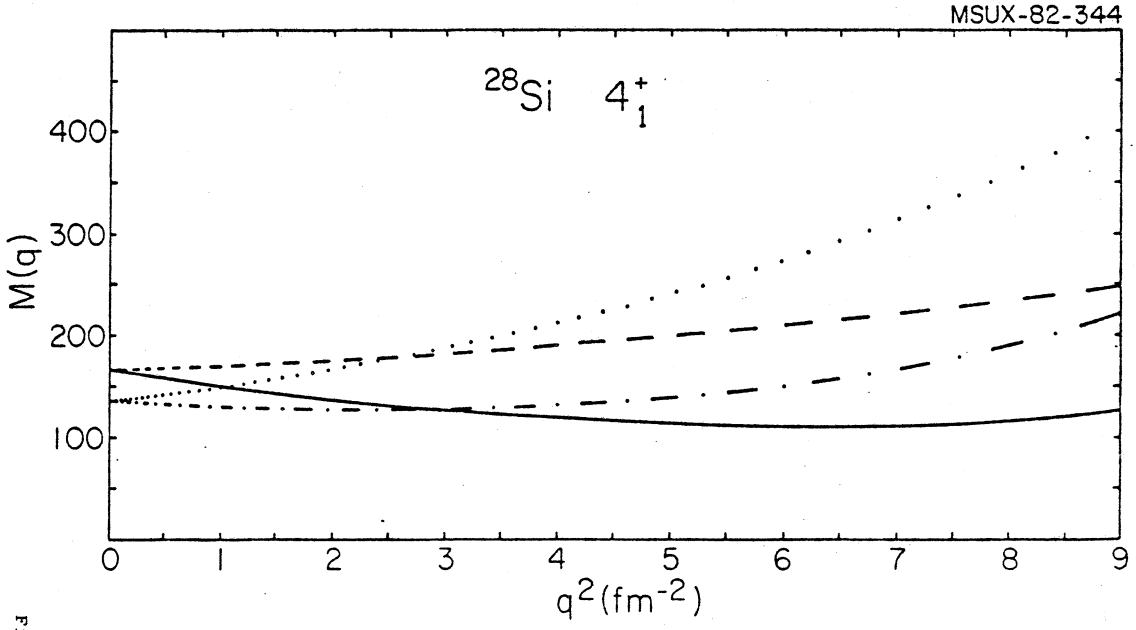

Fig. 6

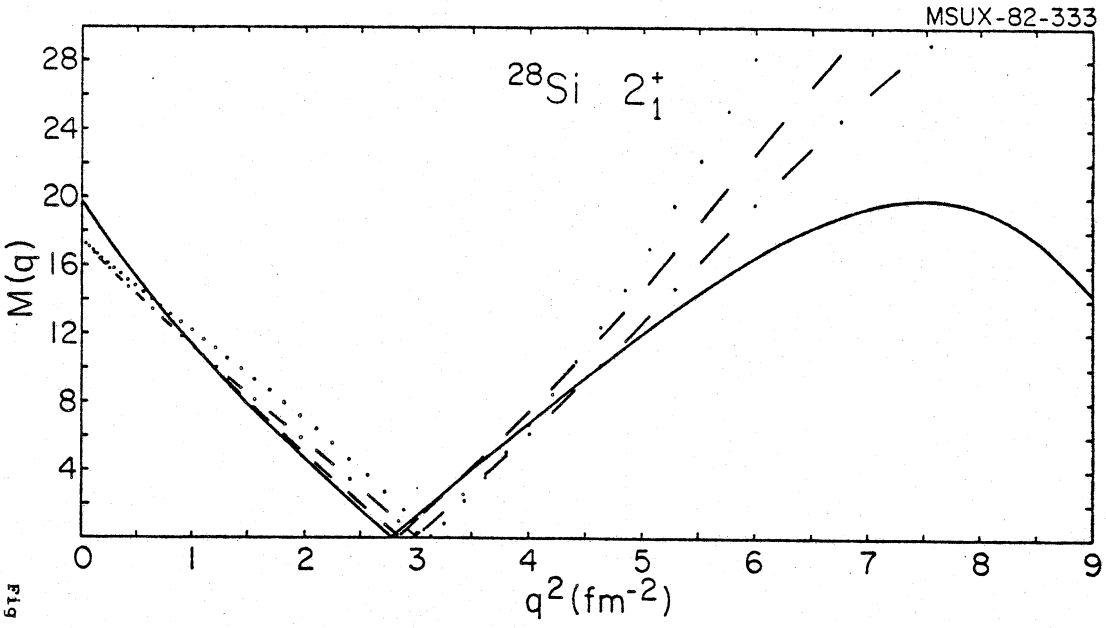
MSUX-82-333
^{28}Si 2_1^+
M(q)
$q^2(fm^{-2})$
28
24
20
16
12
8
4
0
1
2
3
4
5
6
7
8
9

Fig 7

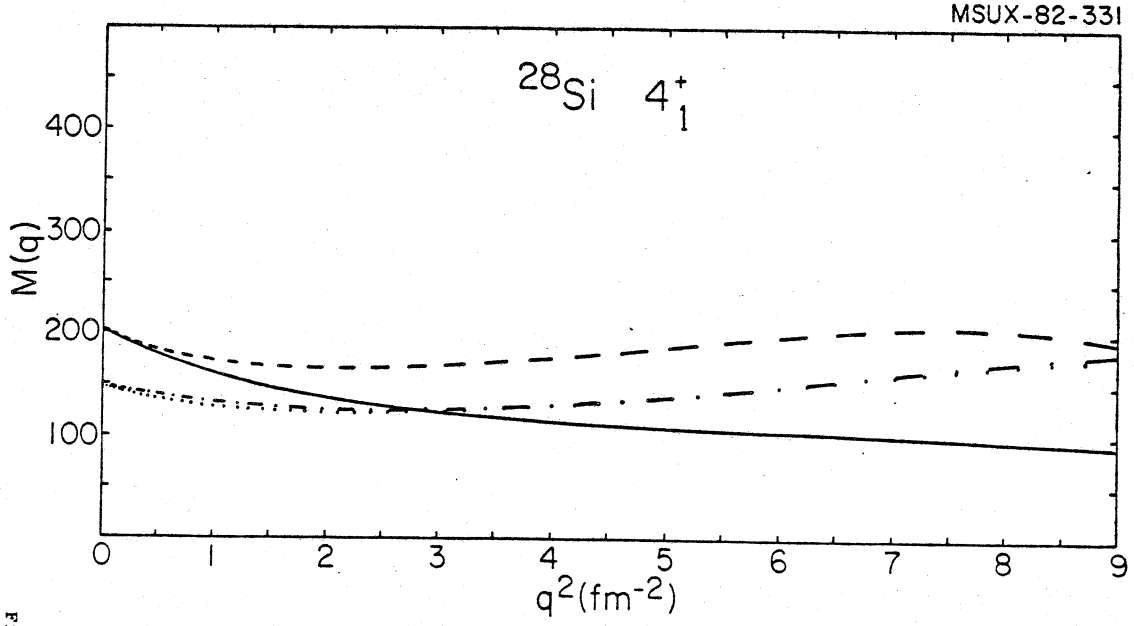
MSUX-82-331
^{28}Si 4_1^+
M(q)
$q^2(fm^{-2})$
400
300
200
100
0
1
2
3
4
5
6
7
8
9

Fig 8

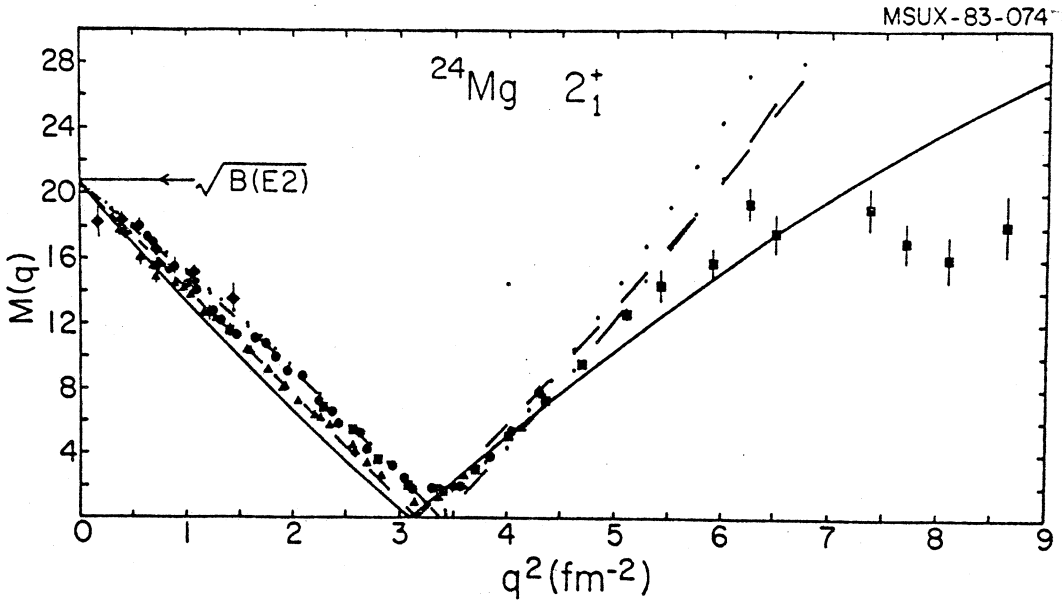
MSUX-83-074
^{24}Mg 2_1^+
$\sqrt{B(E2)}$
M(q)
$q^2(fm^{-2})$

Fig. 9

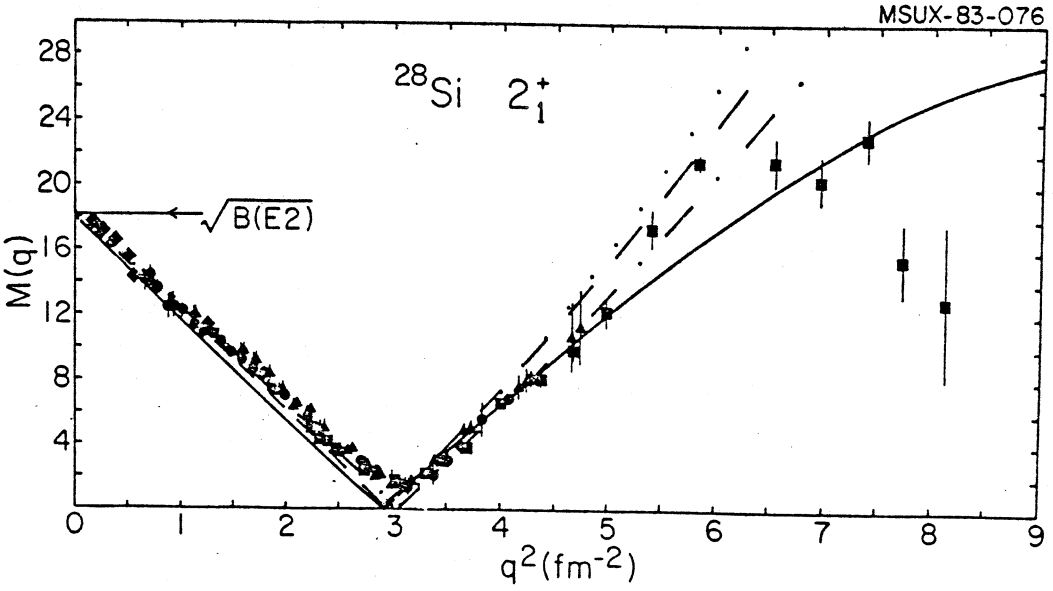
MSUX-83-076
^{28}Si 2_1^+
$\sqrt{B(E2)}$
M(q)
$q^2(fm^{-2})$

Fig. 10

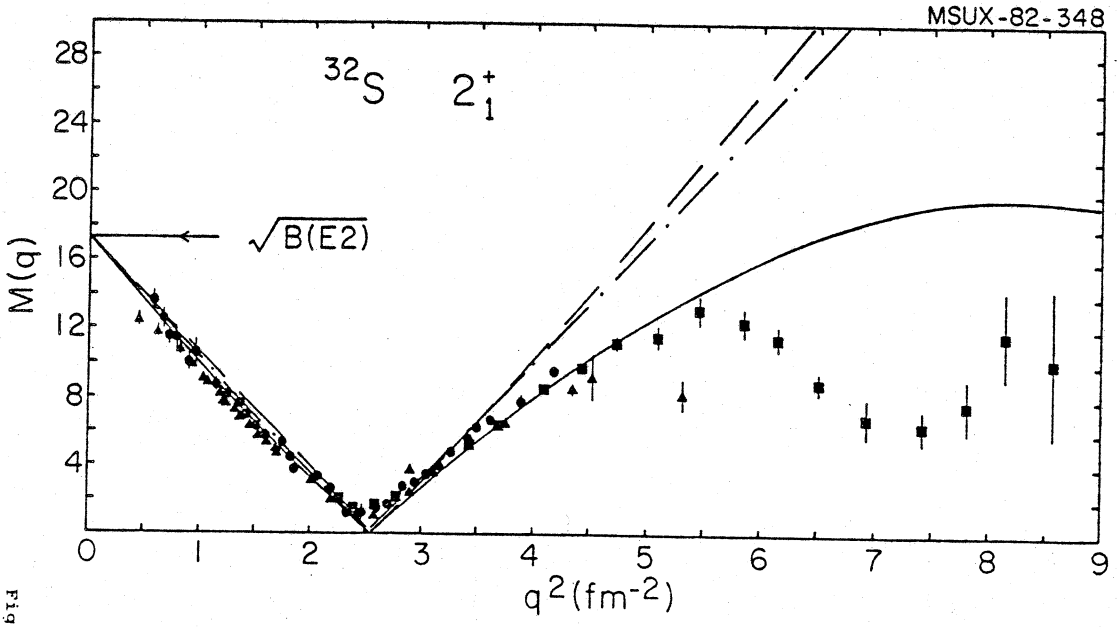
MSUX-82-348
^{32}S 2_1^+
$\sqrt{B(E2)}$
M(q)
$q^2(fm^{-2})$
28
24
20
16
12
8
4
0
1
2
3
4
5
6
7
8
9

Fig 11

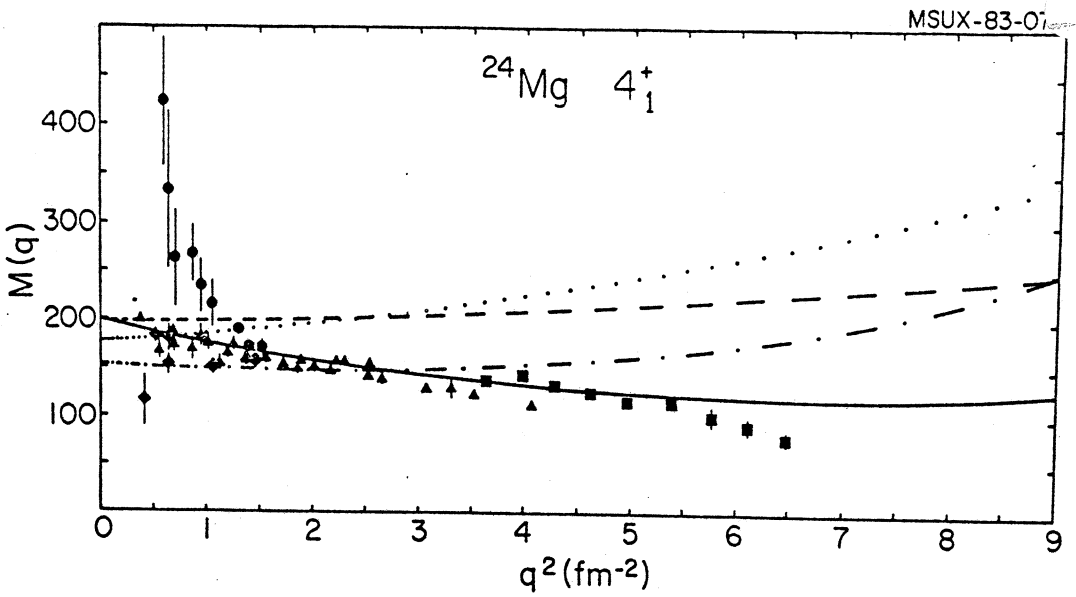
MSUX-83-07
^{24}Mg 4^+_1
M(q)
400
300
200
100
0
1
2
3
4
5
6
7
8
9
$q^2(fm^{-2})$

Fig. 12

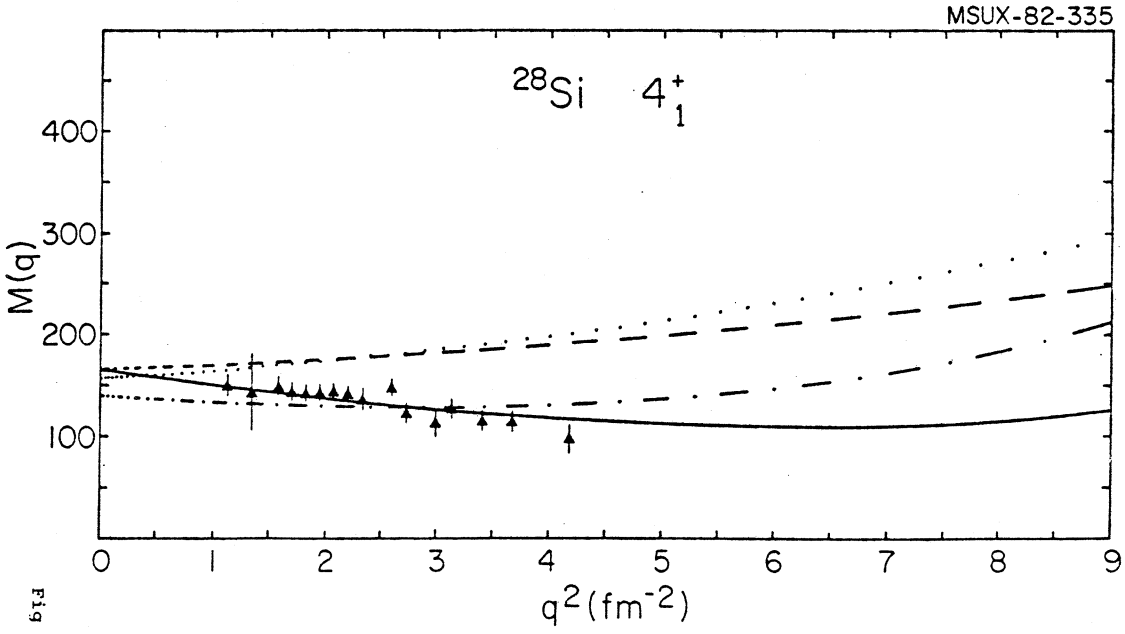
MSUX-82-335
^{28}Si 4^+_1
M(q)
400
300
200
100
0
1
2
3
4
5
6
7
8
9
$q^2(fm^{-2})$

Fig 13

MSUX-83-072

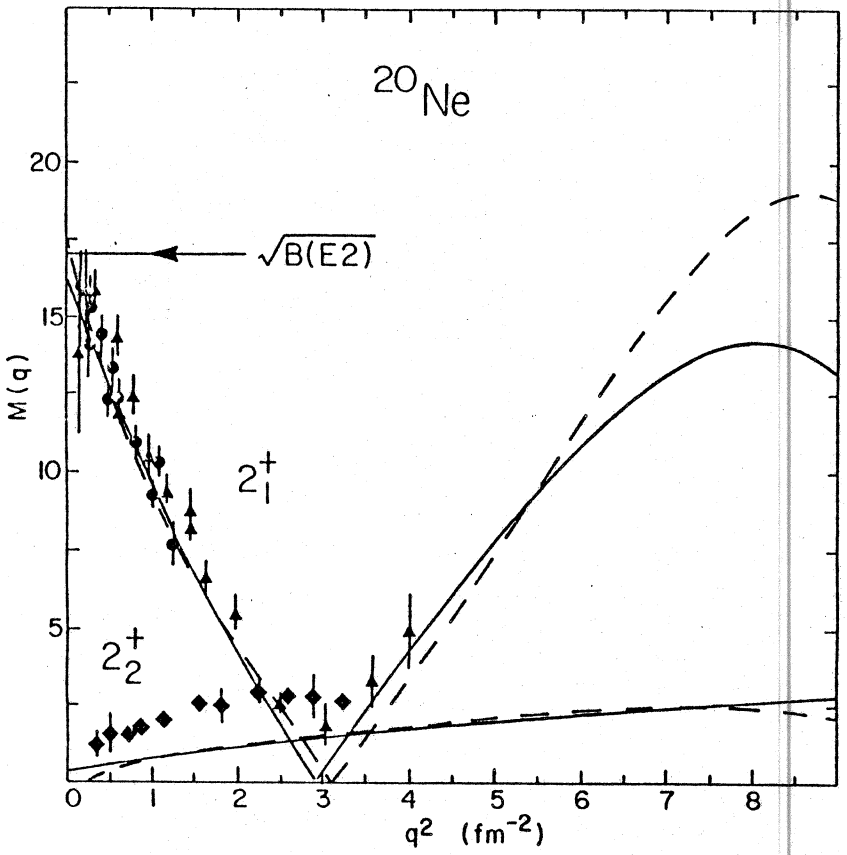

Fig. 14

MSUX-82-334

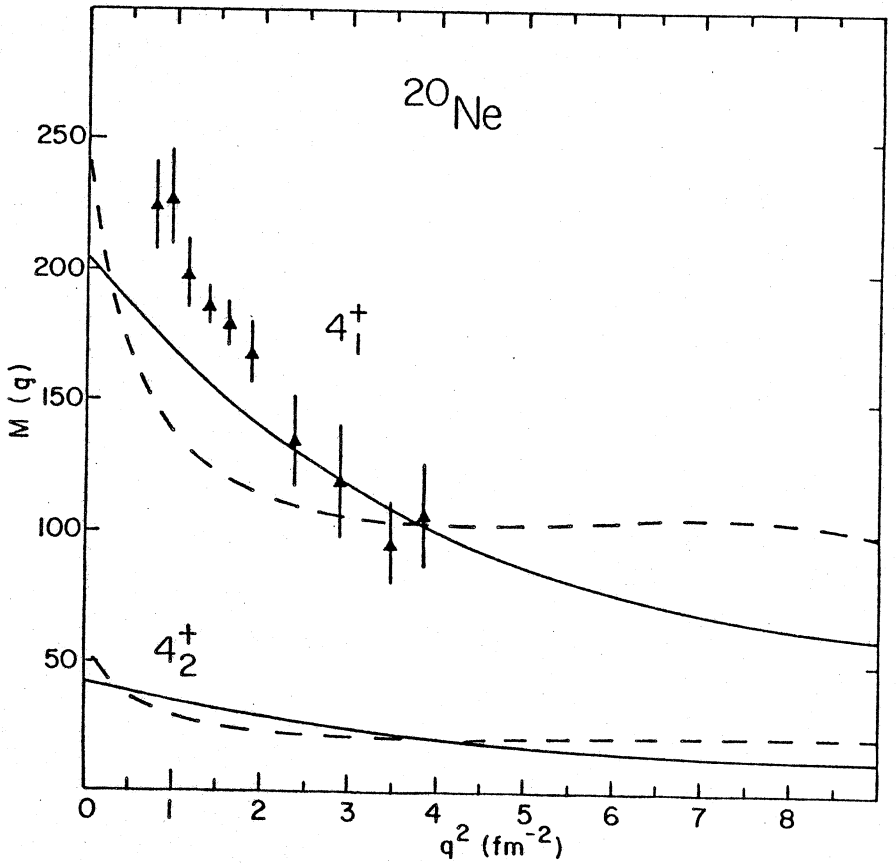

Fig 15

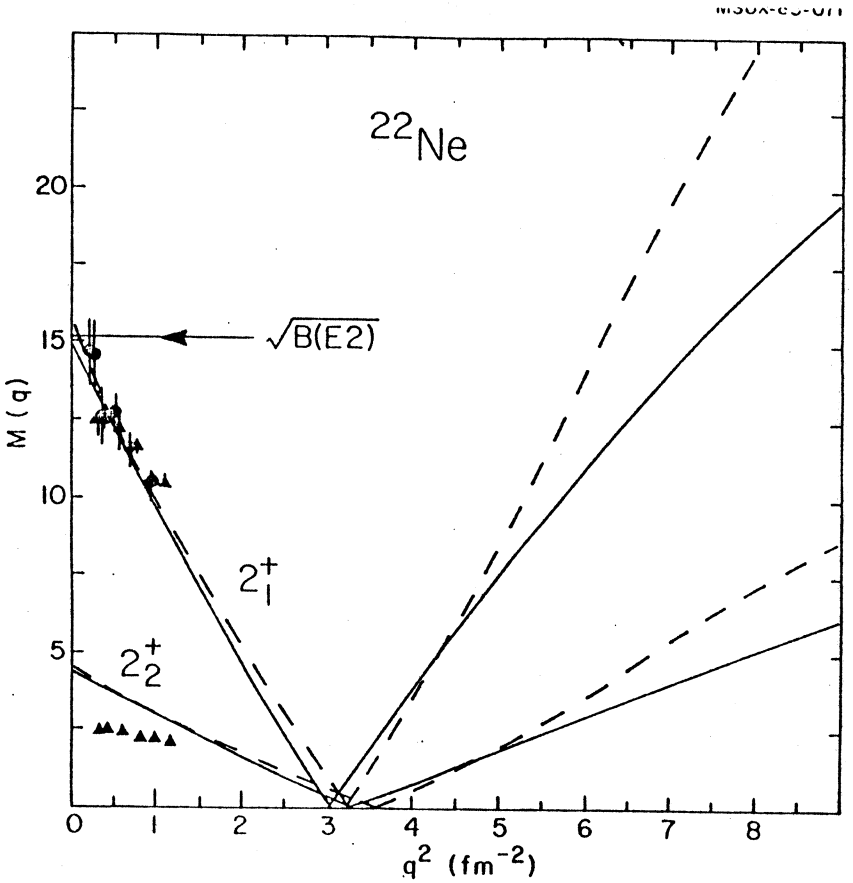

Fig. 16

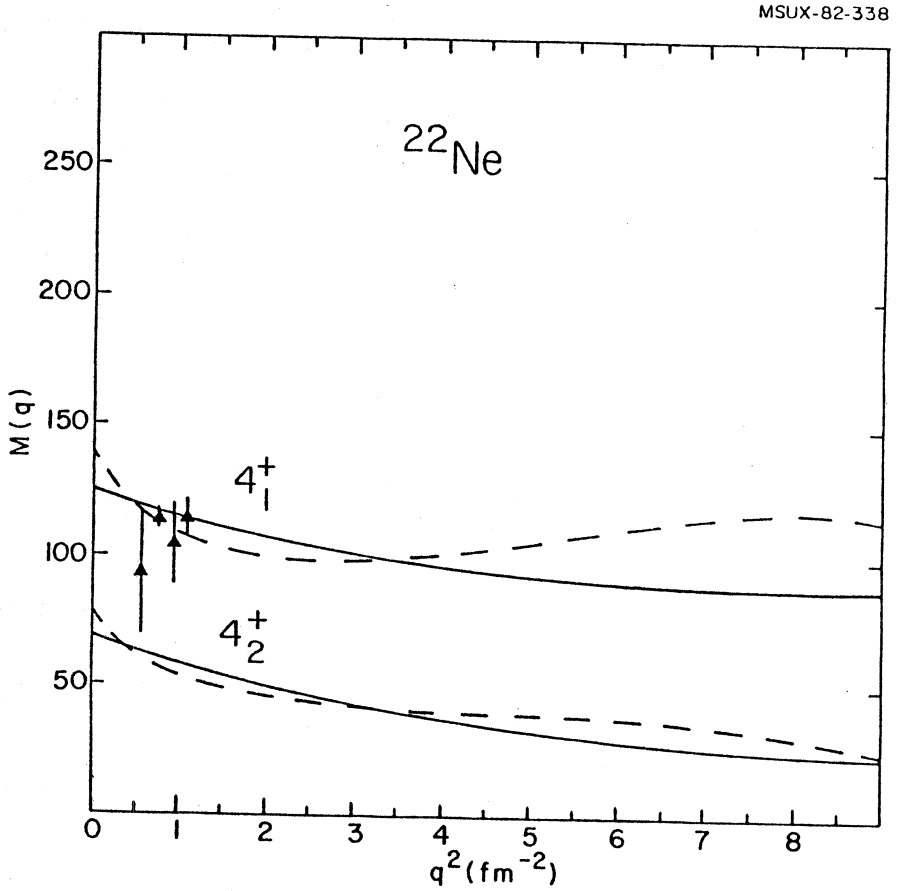

Fig 17

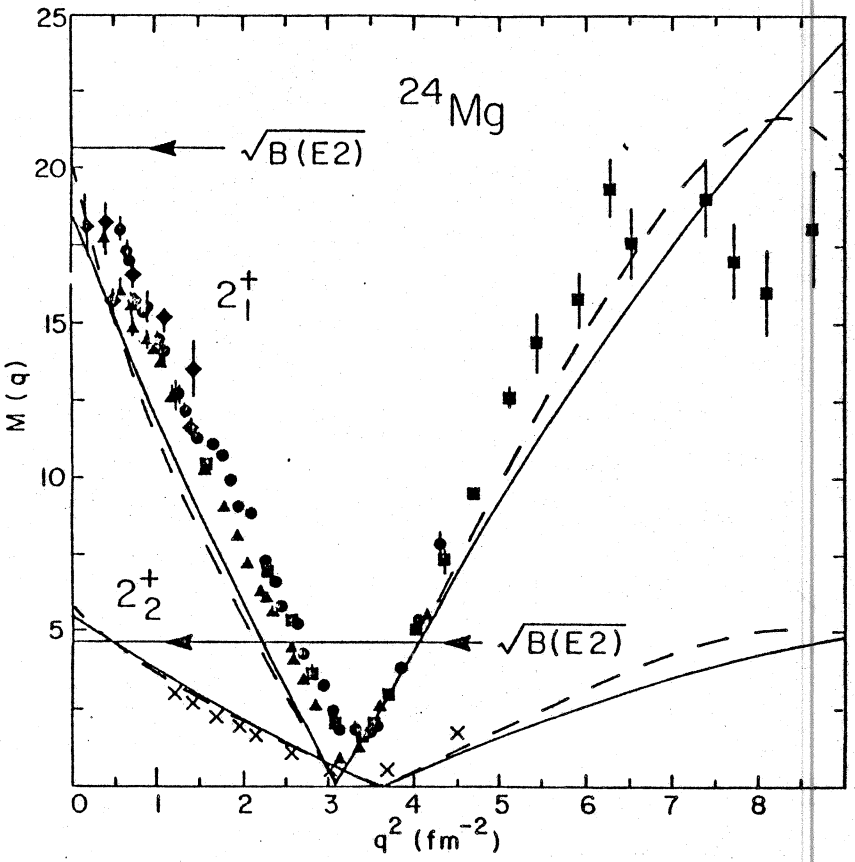

Fig. 18

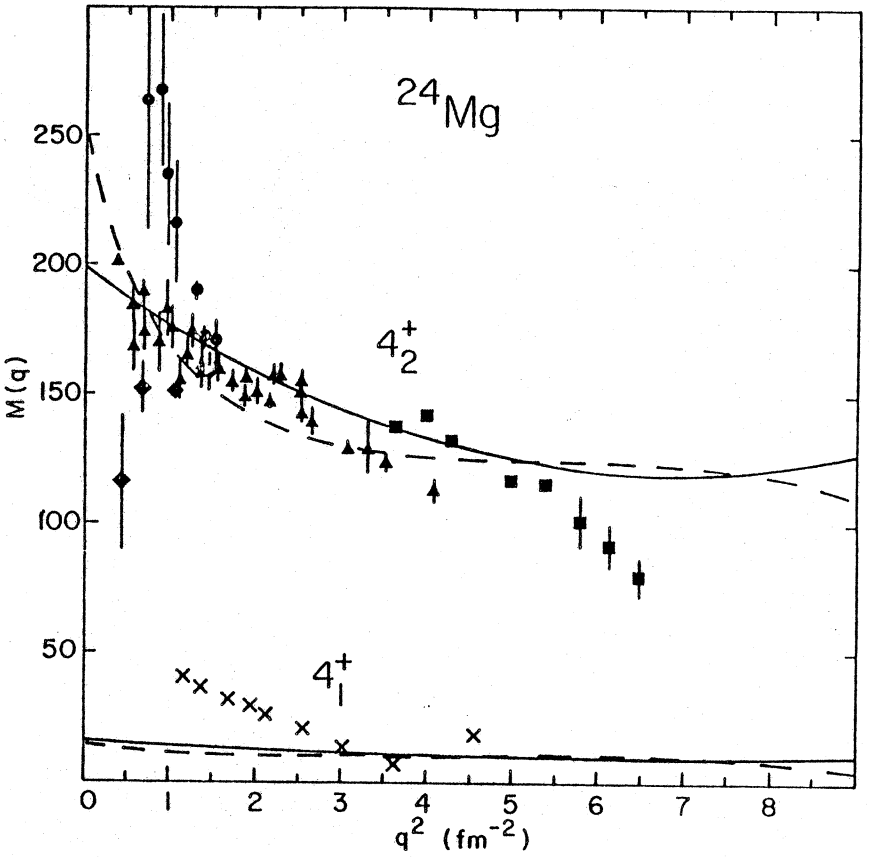

Fig. 19

MSUX-83-069

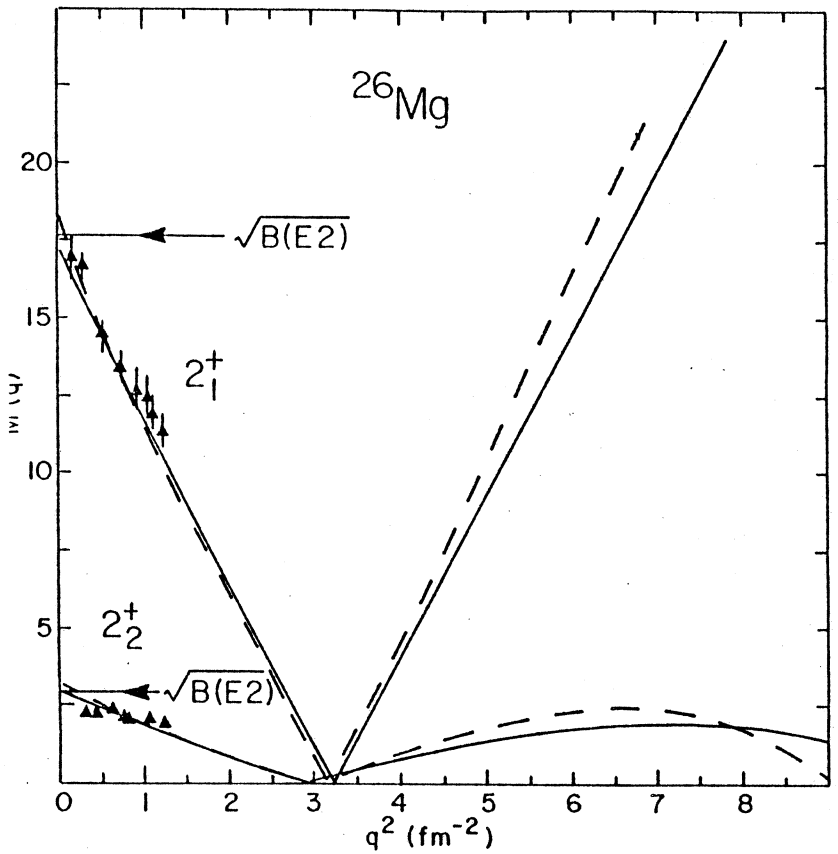

Fig. 20

MSUX-83-068

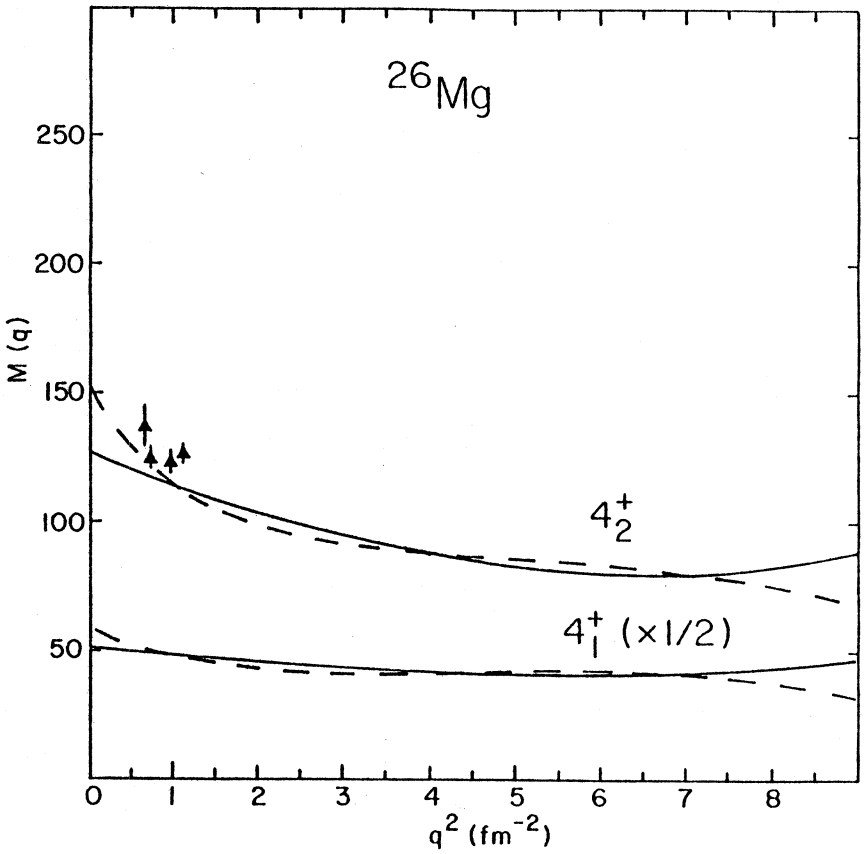

Fig. 21

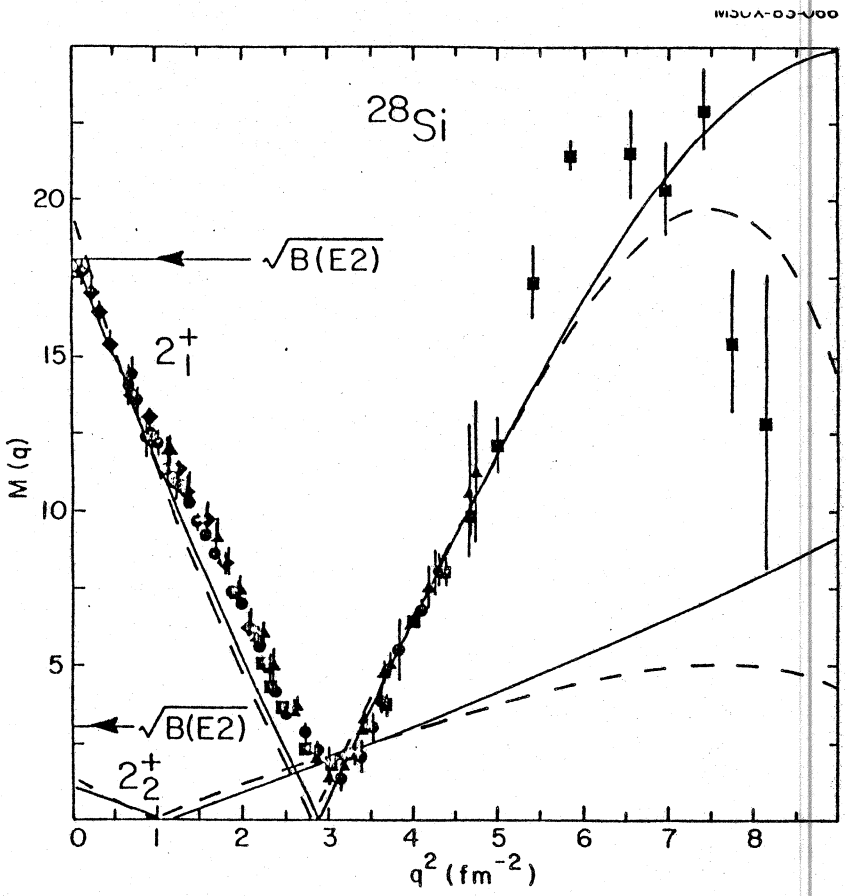
MSUX-83-066
^{28}Si
$\sqrt{B(E2)}$
2_1^+
$\sqrt{B(E2)}$
2_2^+
M (q)
q^2 (fm^{-2})

Fig. 22

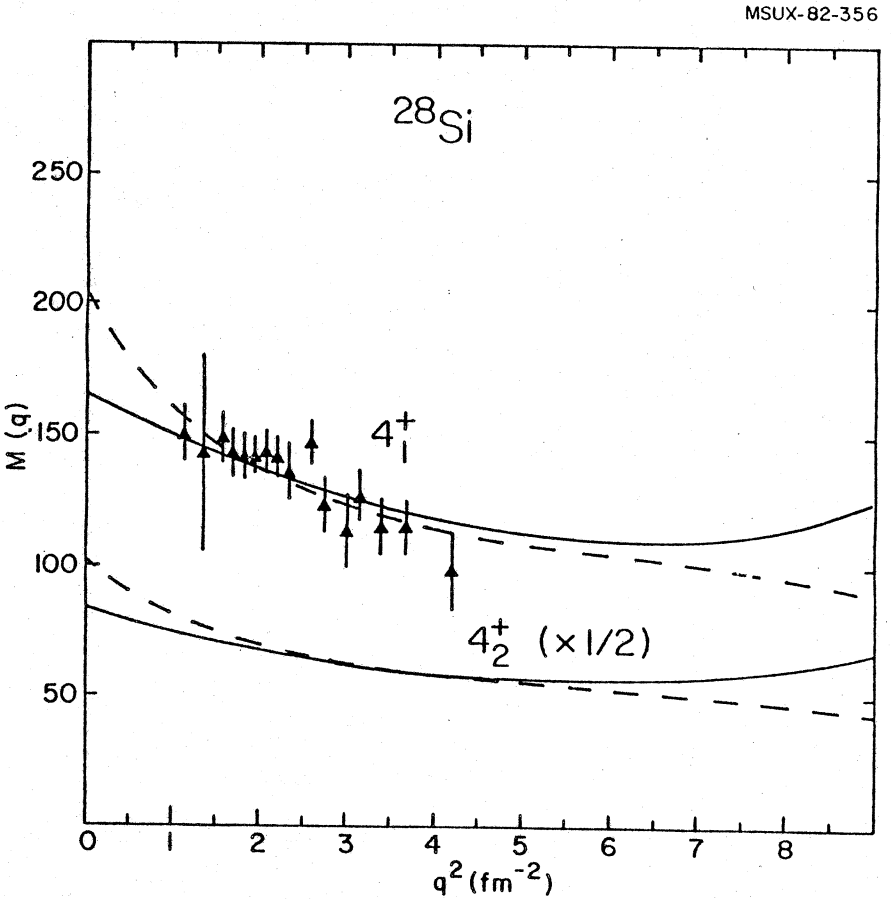
MSUX-82-356
^{28}Si
4_1^+
4_2^+ (×1/2)
M (q)
q^2 (fm^{-2})

Fig 23

MSUX-83-070

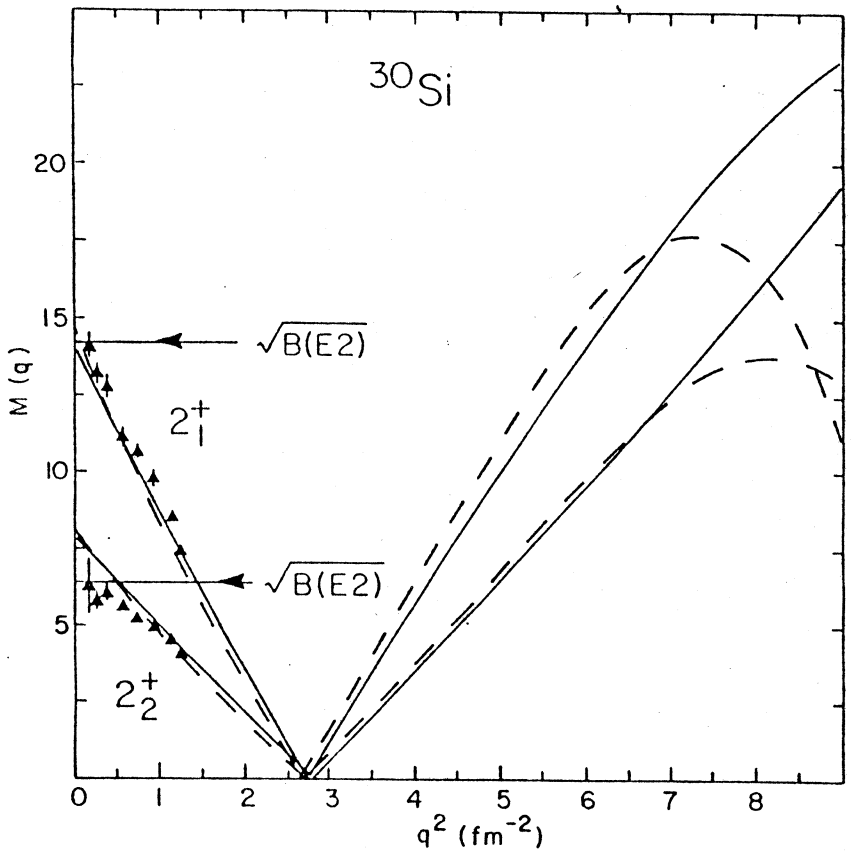

Fig. 24

MSUX-82-378

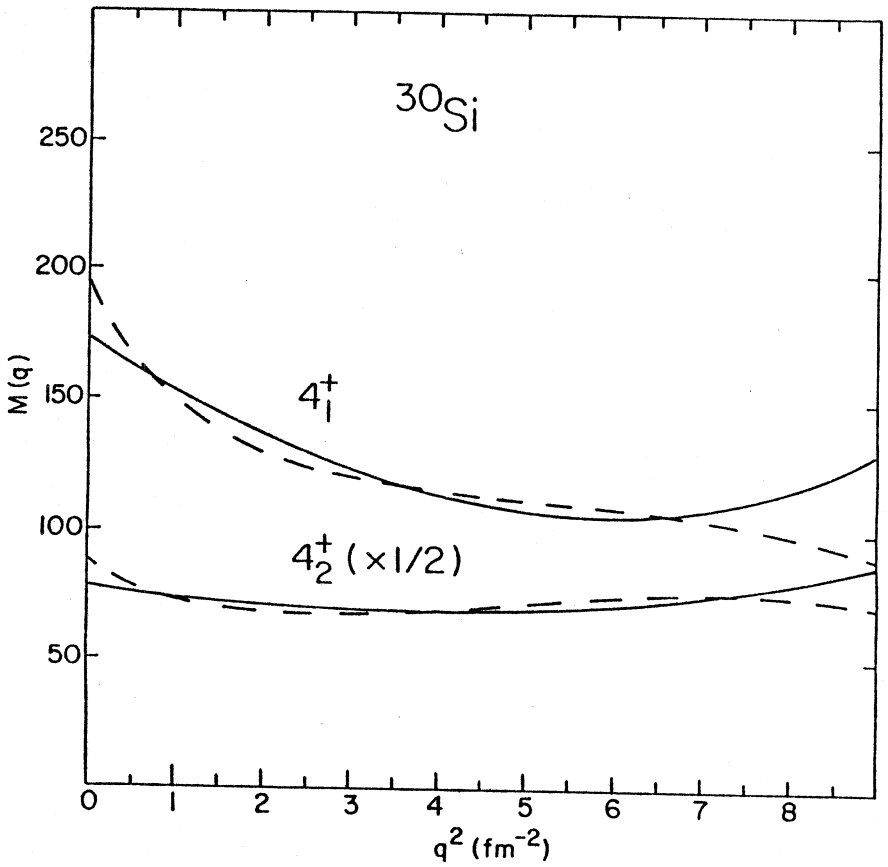

Fig 25

MSUX-82-368

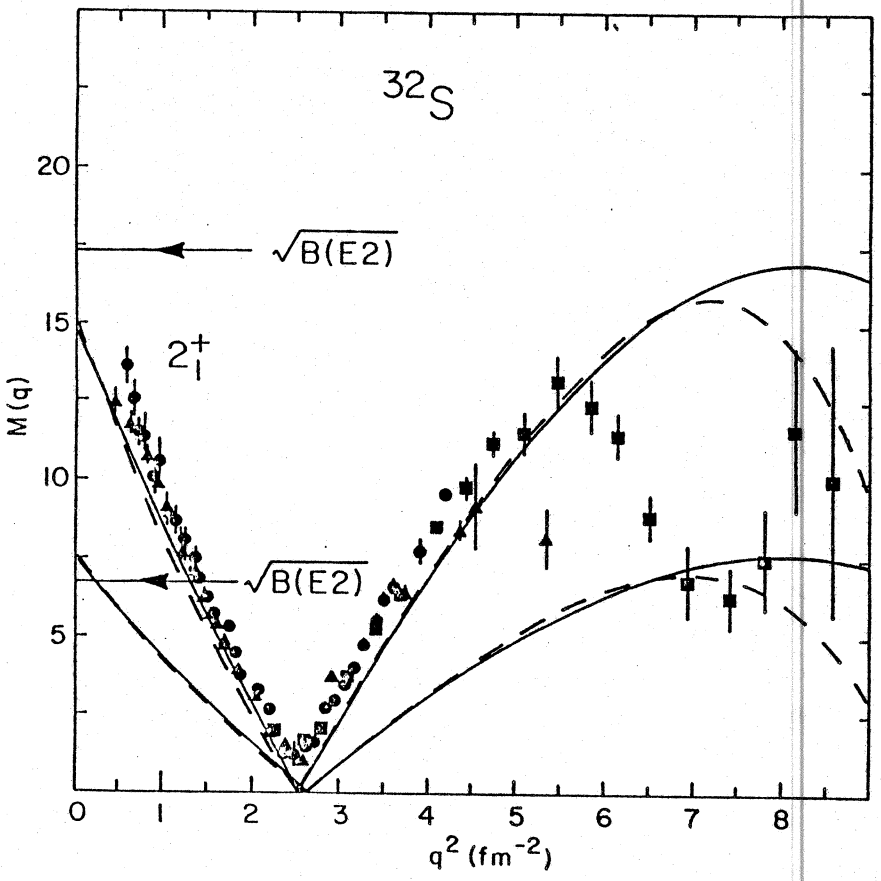

Fig 26

MSUX-82-360

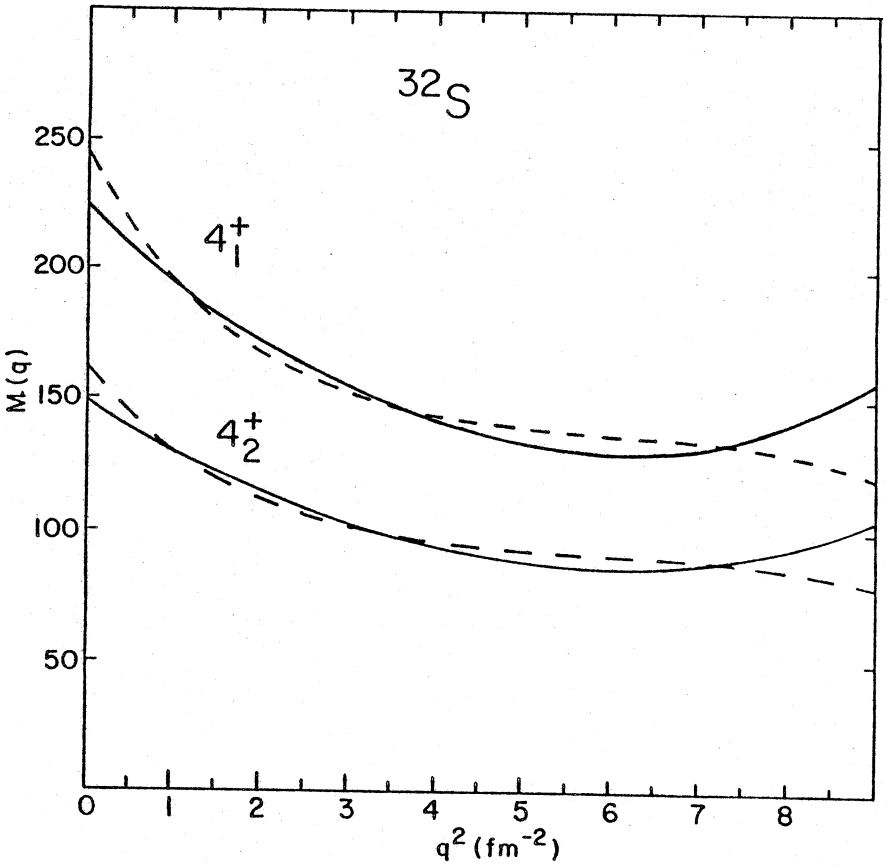

Fig 27

MSUX-82-361

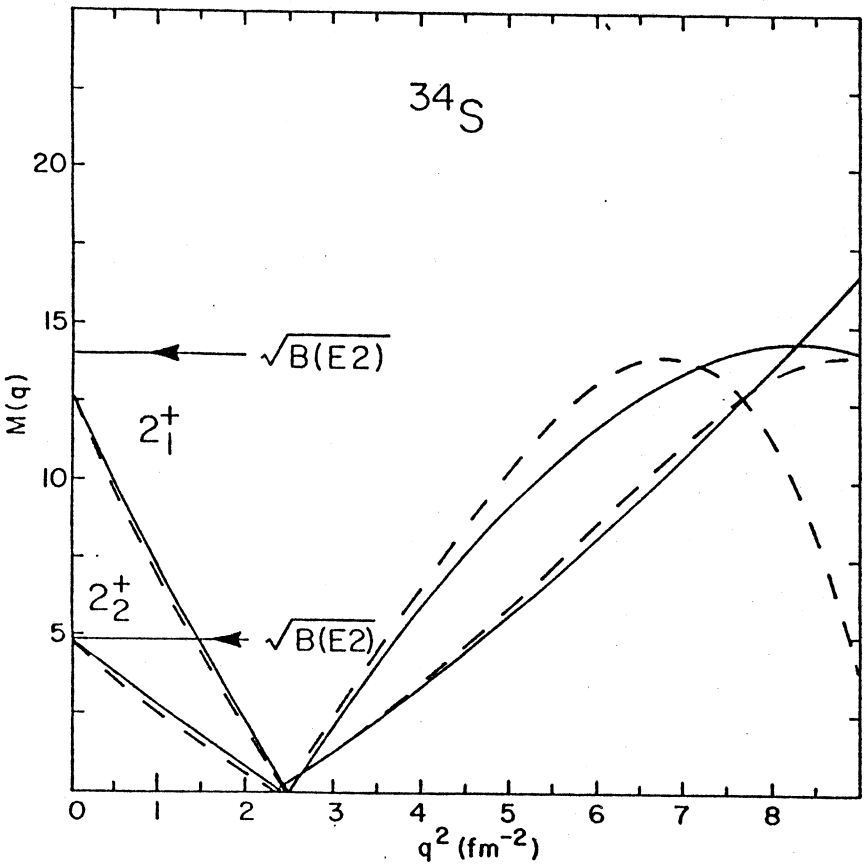

Fig 28

MSUX-82-362

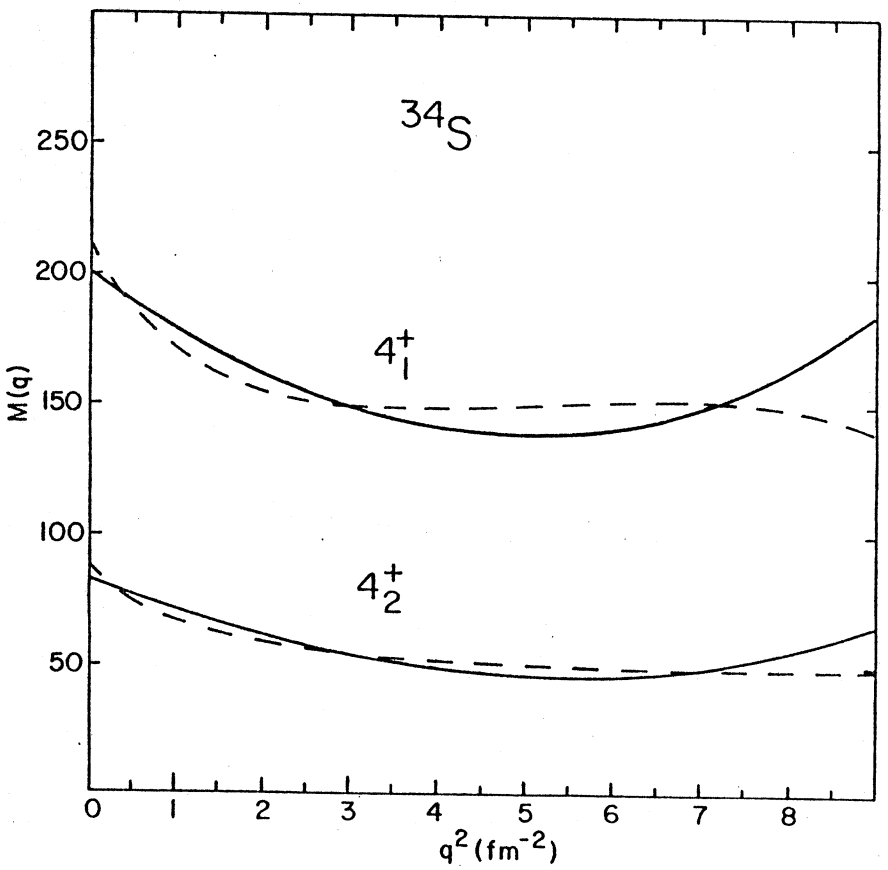

Fig 29

MSUX-82-364

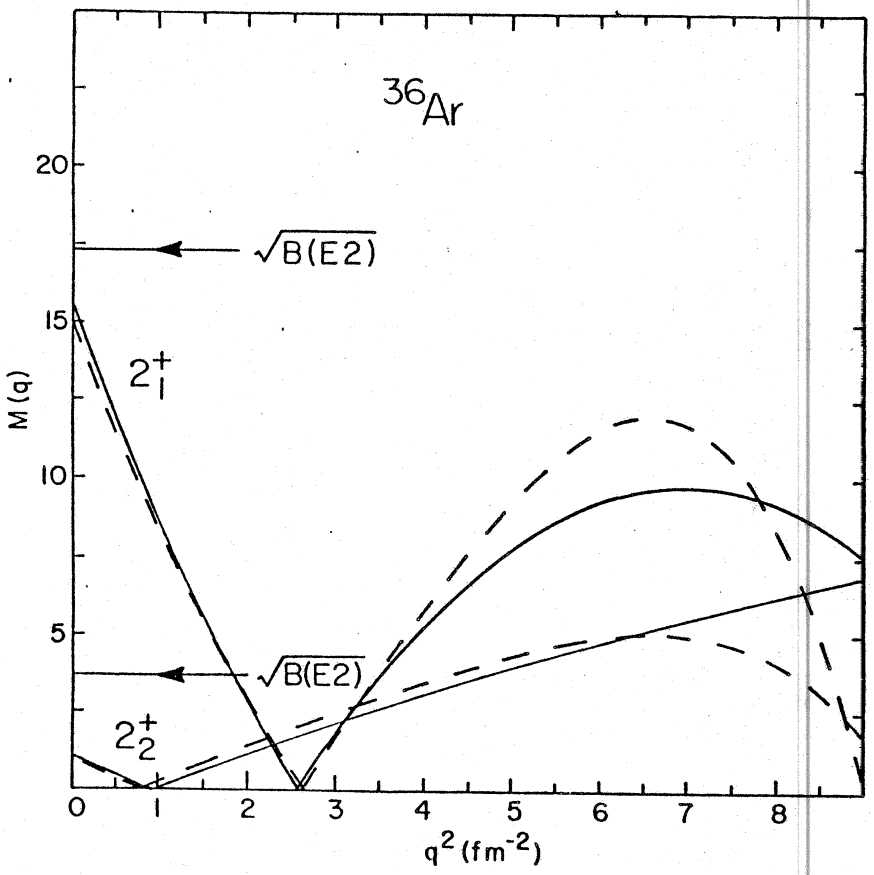

Fig 30

MSUX-82-365

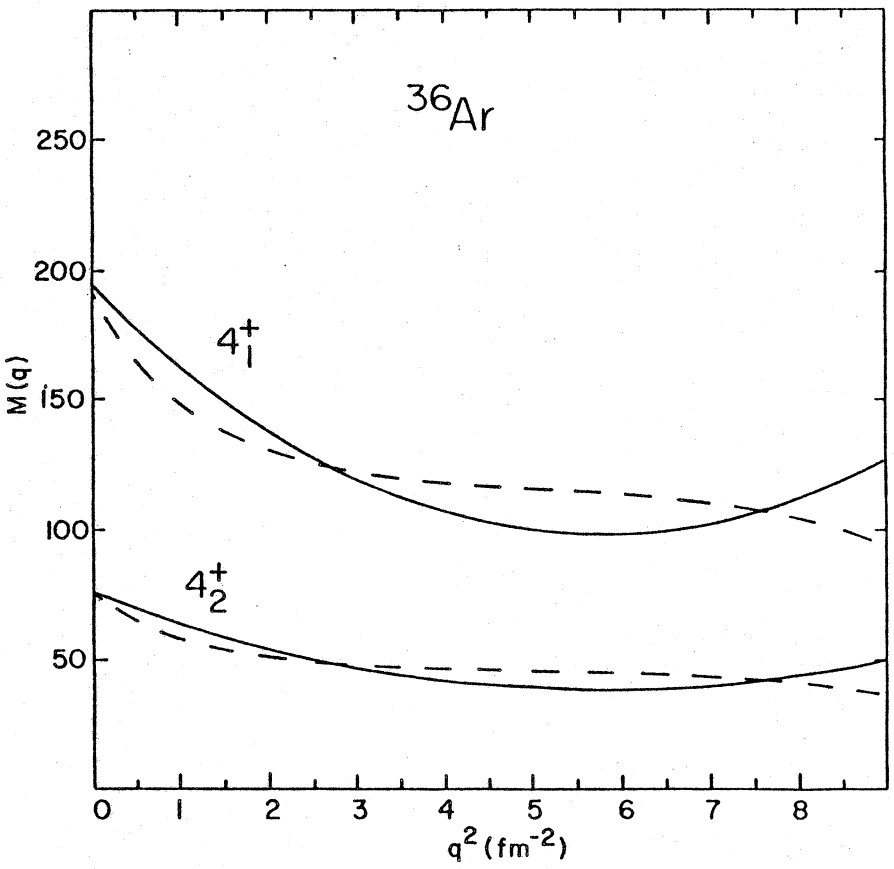

Fig 31